Cell Death and Differentiation (2015) 22, 626–642

www.nature.com/cdd

Regulation of neuronal survival and morphology by the E3 ubiquitin ligase RNF157

A Matz[1,5], S-J Lee[1,5], N Schwedhelm-Domeyer[1,5], D Zanini[2], A Holubowska[1,3], M Kannan[1], M Farnworth[1], O Jahn[3,4], MC Göpfert[2] and J Stegmüller*[,1,3]

Neuronal health is essential for the long-term integrity of the brain. In this study, we characterized the novel E3 ubiquitin ligase ring finger protein 157 (RNF157), which displays a brain-dominant expression in mouse. RNF157 is a homolog of the E3 ligase mahogunin ring finger-1, which has been previously implicated in spongiform neurodegeneration. We identified RNF157 as a regulator of survival in cultured neurons and established that the ligase activity of RNF157 is crucial for this process. We also uncovered that independently of its ligase activity, RNF157 regulates dendrite growth and maintenance. We further identified the adaptor protein APBB1 (amyloid beta precursor protein-binding, family B, member 1 or Fe65) as an interactor and proteolytic substrate of RNF157 in the control of neuronal survival. Here, the nuclear localization of Fe65 together with its interaction partner RNA-binding protein SART3 (squamous cell carcinoma antigen recognized by T cells 3 or Tip110) is crucial to trigger apoptosis. In summary, we described that the E3 ligase RNF157 regulates important aspects of neuronal development.
Cell Death and Differentiation (2015) **22,** 626–642; doi:10.1038/cdd.2014.163; published online 24 October 2014

Neurodegeneration leads to loss of neurons and thus to severe and irreparable damage of the brain. A common histopathological feature in postmortem brains of patients with neurodegenerative diseases such as Parkinson's or Alzheimer's disease is the presence of ubiquitin-laden protein deposits.[1–3] These deposits implicate the ubiquitin proteasome system (UPS) in neurodegeneration. In addition to histopathological clues, genetic evidence demonstrates that erroneous UPS components have detrimental effects on the developing and adult brain resulting in neurodegenerative disorders.[4,5]

The UPS is responsible for the posttranslational modification of proteins by ubiquitin, which requires an enzymatic cascade.[6] The E3 ubiquitin ligases specifically recognize the substrate proteins and mediate their ubiquitination, which can result in their degradation that ensures the homeostasis in cells or in non-proteolytic signaling events.[7,8] The largest group of E3 ligases constitutes the RING (really interesting new gene) ligases, which serve as scaffold proteins to recruit both the substrate and the E2 ubiquitin-conjugating enzyme that binds to the RING domain,[9] facilitating the transfer of ubiquitin from the E2 to the substrate.

Although there are several hundred E3 ligases,[10] only a few have been studied so far in the context of neuronal survival or neurodegeneration.[11–15] Among those, mahogunin ring finger-1 (MGRN1) has been implicated in an age-dependent spongiform encephalopathy characterized in a mouse model.[15]

In this study, we characterized the novel E3 ubiquitin ligase ring finger protein 157 (RNF157), the homolog of MGRN1. We described that RNF157, which is predominantly expressed in the brain, regulates neuronal survival and morphology in cultured neurons. We further identified the adaptor protein APBB1 (amyloid beta precursor protein-binding, family B, member 1 or Fe65) as a substrate and a downstream component in RNF157-regulated neuronal survival. Also, we demonstrated that nuclear Fe65 together with the RNA-binding protein SART3 (squamous cell carcinoma antigen recognized by T cells 3 or Tip110) triggers apoptosis. Taken together, we described that the E3 ligase RNF157 acts in different aspects of neuronal development.

Results

RNF157 is predominantly expressed in the brain. We started out by characterizing the expression of RNF157 at the mRNA and protein level. We found a predominant expression of *Rnf157* mRNA in the brain and little or no expression in non-neural tissues (Figure 1a). To examine the expression of RNF157 at the protein level, we first established the specificity of the RNF157 antibody using antibody–antigen competition for which we generated recombinant rat RNF157 protein that is recognized by the polyclonal RNF157 antibody (Supplementary Figure S1a). Immunoblotting of brain lysates using the RNF157 antibody or antigen-preabsorbed RNF157 antibody revealed that a band of 110 kDa disappeared in the

[1]Cellular and Molecular Neurobiology Group, Max Planck Institute of Experimental Medicine, Göttingen, Germany; [2]Department of Cellular Neurobiology, Schwann-Schleiden Center, Julia Lermontowa Weg 3, University of Göttingen, Göttingen, Germany; [3]Center for Nanoscale Microscopy and Molecular Physiology of the Brain (CNMPB), Göttingen, Germany and [4]Proteomics Group, Max Planck Institute of Experimental Medicine, Göttingen, Germany
*Corresponding author: J Stegmüller, Cellular and Molecular Neurobiology Group, Max Planck Institute of Experimental Medicine, Hermann Rein Strasse 3, Göttingen 37075, Germany. Tel: +49 551 3899 560; Fax: +49 551 3899 201; E-mail: stegmueller@em.mpg.de
[5]These authors contributed equally to this work.
Abbreviations: UPS, ubiquitin proteasome system; RNF157, ring finger protein 157; MGRN1, mahogunin ring finger-1; RING, really interesting new gene; CGNs, cerebellar granule neurons; RNAi, RNA interference; NES, nuclear exclusion sequence; NLS, nuclear localization sequence; NF, nuclear fraction; PNS, postnuclear supernatant; DIV, day *in vitro*; NEM, N-ethylmaleimide; P, postnatal day
Received 26.3.14; revised 19.8.14; accepted 29.8.14; Edited by A Ashkenazi; published online 24.10.14

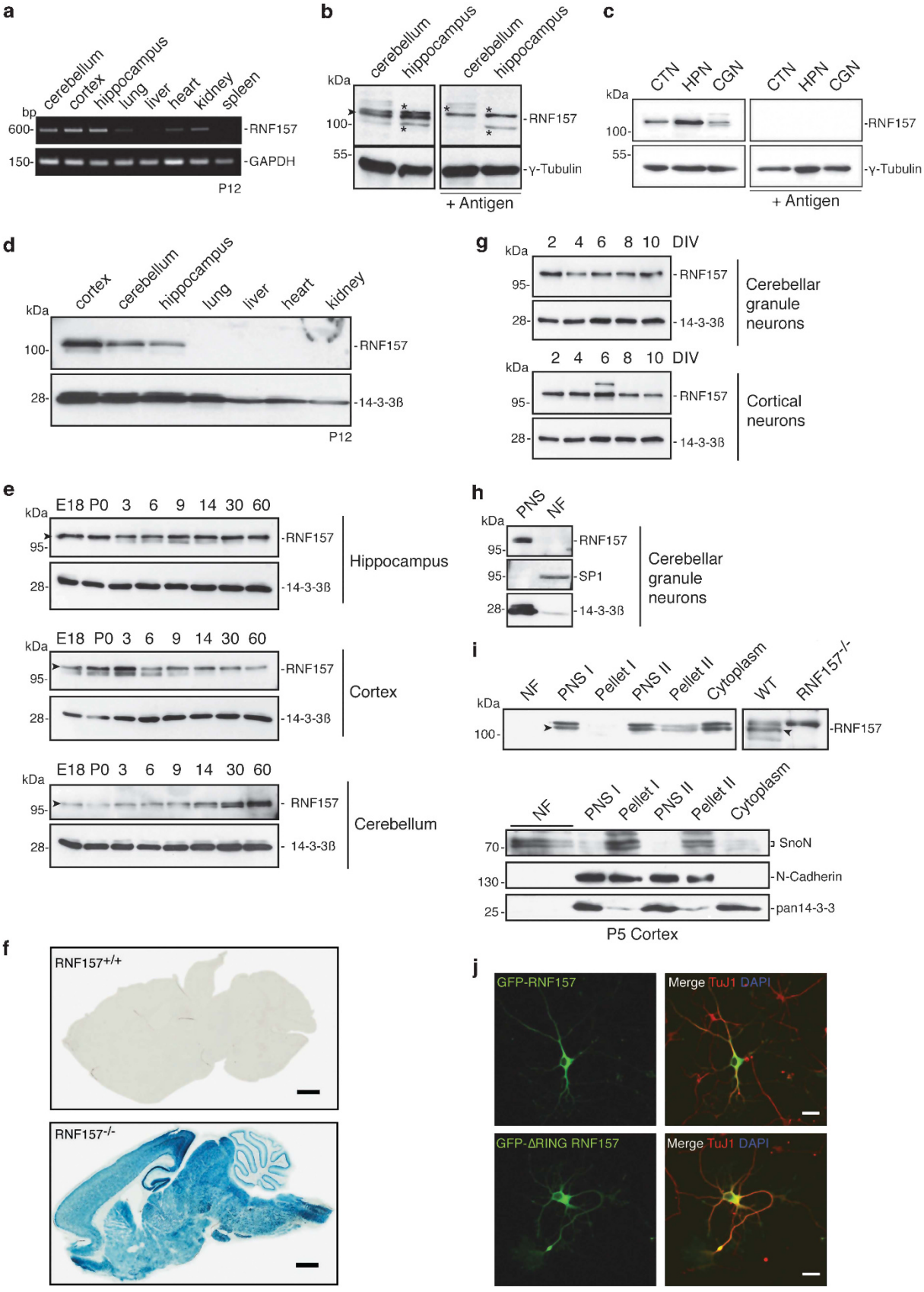

Figure 1 For caption see next page

latter condition (Figure 1b). Also, immunoblotting of lysates from cultured neurons with RNF157 antibody and antigen-preabsorbed RNF157 antibody abolished the 110 kDa band (Figure 1c). The calculated size of rat RNF157 (644 aa; 70 kDa), however, did not match the apparent size of RNF157 in the gel. We then generated a larger recombinant rat RNF157 protein that lacks the RING domain and whose calculated size also did not match the size in the gel (Supplementary Figure S1b). Mass spectrometric analysis, however, revealed the correct size and identity of the recombinant RNF157 (Supplementary Figure S1c). The discrepancy of theoretical and apparent size could be attributed to the relatively high content of acidic amino acids. Although acidic proteins have been reported to migrate more slowly in SDS-PAGE,[16,17] we cannot exclude that the posttranslational modifications contribute to the anomalous running behavior of RNF157. Taken together, these experiments established the specificity of the RNF157 antibody and identified RNF157 as an acidic, 110 kDa protein.

Consistent with the RT-PCR results, immunoblotting demonstrated that RNF157 was predominantly expressed in nervous tissue at postnatal day (P) 12, whereas no expression was detectable in non-neural tissues (Figure 1d). To determine the temporal expression of RNF157 in hippocampus, cortex and cerebellum, we analyzed tissues from embryonic day 18 to P60 and found robust RNF157 expression in hippocampus and cortex and lower expression in the cerebellum (Figure 1e). We also found this expression pattern in a sagittal brain section of an RNF157 knockout mouse (Figure 1f, Supplementary Figures S2a–c). Also, we found robust expression of RNF157 in cultured neurons (Figure 1g).

Interestingly, while RNF157 and the homologous E3 ligase MGRN-1 are encoded by two independent genes in mammals, *Drosophila* has one *RNF157*-like gene (*CG9941*). To assess its expression pattern, we generated transgenic flies and found that CG9941 is restricted to the nervous system both in larvae and adult flies overlapping with the pan-neuronal marker nc82 (bruchpilot) (Supplementary Figures S2d and e). These analyses revealed that RNF157 is evolutionarily conserved and predominantly expressed in the brain.

We then determined the subcellular localization of RNF157 and subjected cerebellar granule neurons (CGNs) to fractionation analysis and found RNF157 in the postnuclear supernatant (PNS) (Figure 1h). With further fractionation analyses using postnatal cortices, we subjected the PNS to ultracentrifugation steps and found that RNF157 was present in the purified cytoplasmic fraction (Figure 1i). To confirm these results, we transfected hippocampal neurons with the GFP-RNF157 plasmid because the RNF157 antibody fails to work in immunocytochemistry. Here, we found GFP-RNF157 evenly distributed in the somatic cytoplasm and processes but absent from the nucleus (Figure 1j). These results identify RNF157 as a cytoplasmic protein.

The E3 ligase RNF157 promotes neuronal survival. Having generated the RNF157 knockout mouse, we did not find any obvious phenotypic differences in young mice (5-day/6-week-old mice). The full analysis of the RNF157 KO mice has only recently been started and is still work in progress. Before generating this mouse, we took an RNA interference (RNAi) approach to determine the function of RNF157 in cultured neurons. To acutely knockdown RNF157, we designed several vector-based small hairpins targeting RNF157 and determined that RNF157 RNAi #3 was most efficient in doing so (Figure 2a). Neither of the RNF157 RNAi constructs induced knockdown of MGRN1 (Supplementary Figure S3a). We also verified the endogenous knockdown of RNF157 in neurons (Figure 2b). When we examined CGNs, transfected at day *in vitro* (DIV) 2 with control vector (U6 promoter in pBluescript) or the RNF157 RNAi #2 and #3 plasmids, we found that acute knockdown of RNF157 with both functional RNF157 RNAi plasmids induced a significant increase in apoptosis, with RNF157 RNAi #3 being more potent (Figure 2c). Also, RNF157 knockdown neurons displayed characteristic signs of apoptosis including pyknotic nuclei, axonal fragmentation and cleaved caspase-3 immunoreactivity (Figure 2d). In contrast to RNF157 RNAi in mammalian neurons, knockdown of the *Drosophila* orthologue CG9941 in the fly brain did not produce any obvious signs of neuronal apoptosis in the brain of young and older flies (Supplementary Figures S3b and c). We then examined if RNF157 supports neuronal survival in other mammalian neuronal cell types. We analyzed hippocampal neurons transfected with control vector or RNF157 RNAi #3 plasmid and found a similar apoptotic response in RNF157 knockdown neurons (Figure 2e). We next induced RNF157 knockdown in neurons of organotypic cortical slices and found that RNF157 RNAi #3 significantly induced apoptosis as compared with control conditions

Figure 1 RNF157 is predominantly expressed in the brain. (**a**) cDNA of indicated tissues isolated from P12 rats were subjected to PCR analysis with RNF157- and GAPDH-specific primers. The latter served as loading control. (**b**) Cerebellar and hippocampal lysates from P12 rats were subjected to immunoblotting with the RNF157 antibody, the RNF157 antibody preabsorbed with RNF157 antigen or the γ-tubulin antibody. The latter served as loading control. Arrowhead indicates specific RNF157 band. Asterisks indicate nonspecific bands. (**c**) Lysates of cultured cortical (CTN), hippocampal (HPN) and CGNs were immunoblotted with the RNF157 antibody, the RNF157 antibody preabsorbed with RNF157 antigen or the γ-tubulin antibody. The latter served as loading control. (**d**) Lysates of indicated neural and non-neural rat tissues were immunoblotted with the RNF157 or the 14-3-3β antibody. The latter served as loading control. (**e**) Lysates of rat cortex, cerebellum and hippocampus isolated at embryonic day (E) 18 to P60, were immunoblotted with the RNF157 or the 14-3-3β antibodies. The latter served as loading control. (**f**) Sagittal vibratome sections from P28 wild-type and RNF157 $-/-$ mice, in which the *Rnf157* gene was interrupted by a gene trap cassette encoding β-Geomycin, were subjected to X-Gal staining. Scale bar equals 1 mm. (**g**) Lysates of CGNs and cortical neurons, cultured for indicated days (DIV), were immunoblotted with the RNF157 or the 14-3-3β antibodies. The latter served as loading control. (**h**) Lysates of CGNs were subjected to subcellular fractionation and immunoblotted with the RNF157, 14-3-3β and SP1 antibodies. The latter two served as quality control for PNS and NF, respectively. (**i**) P5 cortex was lysed and fractionated into NF and PNS. The PNS was further processed by ultracentrifugation to remove plasma membrane and heavy membrane components, resulting in PNS I, PNS II, pellet I and II and the cytoplasmic fraction. These fractions were immunoblotted with the RNF157, SnoN (NF), pan14-3-3 (cytoplasmic fraction) and N-Cadherin (plasma membrane marker) antibodies. Lysates of wild-type and RNF157 $-/-$ brains were used as positive control for the specific RNF157 band indicated by arrowhead. (**j**) Hippocampal neurons were transfected with the GFP-RNF157 expression plasmid, subjected to immunostaining with the GFP and the neuronal marker TuJ1 antibodies (class III β-tubulin) and analyzed with confocal microscopy. Scale bar = 20 μm

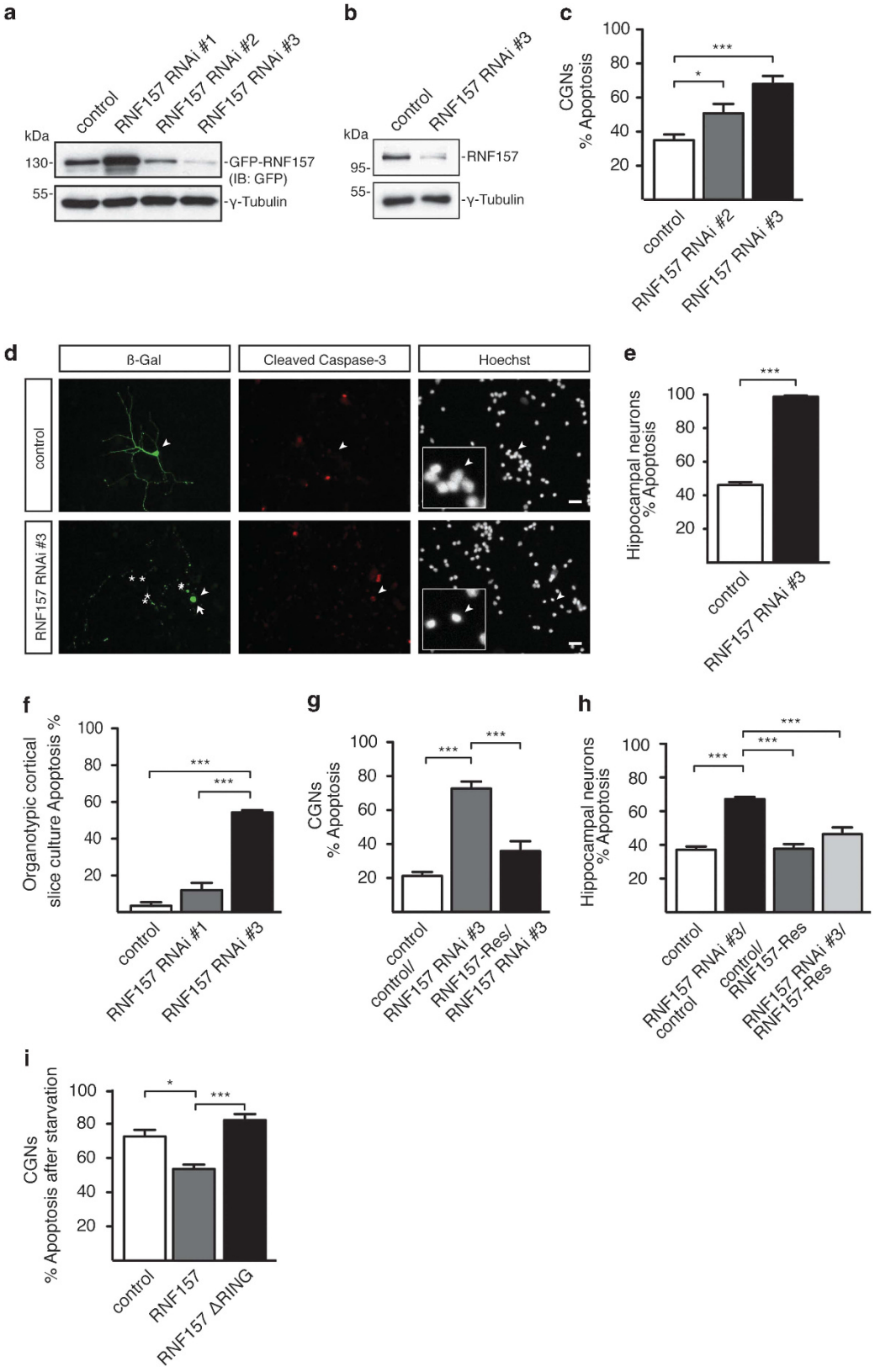

Figure 2 For caption see next page

(Figure 2f, Supplementary Figure S3d). These results indicate that RNF157 promotes survival in mammalian neurons.

To ensure the specific phenotype of RNF157 knockdown and to rule out off-target effects, we constructed and validated an RNF157 RNAi-resistant RNF157-Rescue (Res) plasmid (Supplementary Figures S3e and f). Subsequent rescue experiments in CGNs, in which the RNF157-Res plasmid was expressed together with RNF157 RNAi, demonstrated a significantly lower apoptotic rate as compared to RNF157 knockdown neurons (Figure 2g). In a similar experiment, we confirmed the full rescue of RNF157 knockdown-induced cell death in hippocampal neurons (Figure 2h). To underscore that RNF157 promotes neuronal survival, we investigated if overexpression of RNF157 protects CGNs from apoptosis. We exposed control-transfected (pCMVmyc) or RNF157-overexpressing CGNs to serum/KCl withdrawal to induce apoptosis. Remarkably, we found that RNF157-expressing neurons displayed significant resistance to serum/KCl withdrawal (Figure 2i). We also determined whether neuronal survival is dependent on the E3 ligase activity of RNF157 and transfected the neurons with the RNF157 ΔRING mutant, in which the RING domain is deleted to abolish ligase activity. Here we found that unlike wild-type RNF157, expression of the RNF157 ΔRING mutant did not result in a decrease of apoptosis (Figure 2i). These data support the notion that RNF157 is promoting survival in an E3 ligase-dependent manner in cultured neurons.

RNF157 supports dendrite growth and maintenance independent of its E3 ligase activity. To investigate further RNF157 functions in neurons, we transfected CGNs with control vector or RNF157 RNAi #2 and #3 plasmids at a time when neuronal polarity is fully established. To prevent morphological effects because of compromised cellular health upon RNF157 knockdown, we co-transfected a plasmid encoding Bcl-XL, which promotes survival without affecting neuronal morphology.[18] We then subjected transfected CGNs to morphological analyses, which revealed that RNF157 knockdown led to reduced total dendritic length as compared to control neurons (Figures 3a and b). The length of the axon (longest process), however, remained unaffected (Figure 3c). As a consequence of reduced total dendritic length, RNF157 RNAi neurons harbored much simpler dendritic arbors (Figure 3d). When we monitored dendrite development and stability for several days, we found that loss of RNF157 led to a destabilization and shrinkage of previously established dendrites (Figure 3e). To ensure the specific dendritic phenotype of RNF157 knockdown, we carried out rescue experiments, which revealed that expression of the RNF157 rescue plasmid upon RNF157 knockdown restored dendrites (Figure 3f). In gain-of-function experiments, we addressed whether overexpression of RNF157 has the opposite effect on dendrite length. We transfected neurons with the control vector or the RNF157 expression plasmid and found that RNF157 overexpression resulted in exuberant dendritic growth (Figures 3g and h). Interestingly, expression of RNF157 ΔRING induced an equally strong increase in dendritic growth (Figures 3g and h). Accordingly, RNF157 overexpression resulted a more complex dendritic arborization (Figure 3i). To examine whether the dendrite-stabilizing function of RNF157 holds true in other types of neurons, we induced RNF157 knockdown in hippocampal neurons and found very small dendritic trees, while axonal lengths were unaffected (Figures 3j–l). Collectively, these data indicate that RNF157 supports growth and maintenance of dendrites independent of its E3 ligase activity in cultured neurons.

The adaptor protein Fe65 interacts with RNF157. To delineate a mechanism by which the E3 ligase RNF157 operates in neurons, we carried out a yeast two-hybrid analysis using a fetal human brain library. Here, we identified the adaptor protein Fe65 (or APBB1) as an interactor of RNF157. Fe65, Fe65-L1 and Fe65-L2 constitutes the Fe65 adaptor protein family,[19,20] of which only Fe65 displays a brain-dominant expression.[20]

To validate the interaction of Fe65 and RNF157, we carried out immunoprecipitation experiments and found that Fe65 robustly associated with RNF157 (Figure 4a). In a reciprocal co-immunoprecipitation, we confirmed this interaction (Supplementary Figure S4a). To establish their interaction in the brain, we first demonstrated that the Fe65 antibody immunoprecipitated Fe65 from brain tissue (Supplementary Figure S4b). In subsequent co-immunoprecipitation analyses, we found that RNF157 and Fe65 interacted endogenously in the brain (Figure 4b,Supplementary Figure S4c).

Figure 2 RNF157 promotes neuronal survival. (**a**) Lysates of HEK293T cells, transfected with the GFP-RNF157 plasmid together with control vector or plasmids encoding RNF157 RNAi #1, #2 or #3, were immunoblotted with the GFP or γ-tubulin antibodies. The latter served as loading control. (**b**) Cortical neurons were mixed with control vector or RNF157 RNAi #3 plasmid and subjected to electroporation using the Amaxa nucleofector. After 5 days in culture, lysates of neurons were immunoblotted with the RNF157 or the γ-tubulin antibodies. The latter served as loading control. (**c**) CGNs, transfected at DIV2 with control vector or plasmids encoding RNF157 RNAi #2 or #3 together with the β-Gal expression plasmid, were subjected to immunocytochemistry at DIV6 with the β-Gal antibody and the nuclear dye bisbenzimide Hoechst 33258. A total of 1225 neurons from three independent experiments were included in the analysis (ANOVA, $^{*}P<0.05$, $^{***}P<0.001$, mean +S.E.M.). (**d**) Representative neurons from **2c**, which were co-stained with β-Gal and cleaved caspase-3 antibodies together with the DNA dye bisbenzimide (Hoechst). Arrowheads indicate transfected neurons. Insets show higher magnification of Hoechst-stained nuclei. Asterisks indicate apoptotic bodies, arrowheads indicate transfected neurons and arrow indicates pyknotic nucleus. Scale bar equals 20 μm. (**e**) Hippocampal neurons, transfected at DIV2 with control vector or a plasmid encoding RNF157 RNAi #3 together with the β-Gal expression plasmid, were analyzed as described in **2c**. A total of 655 neurons from three independent experiments were included in the analysis (Student's *t*-test, $^{***}P<0.001$, mean +S.E.M.). (**f**) Organotypic slice cultures from P0 cortex were transfected at DIV2 with control vector, RNF157 RNAi #1 or #3 and analyzed at DIV6. A total of 217 neurons from three independent experiments were included in the analysis (ANOVA, $^{***}P<0.001$, mean +S.E.M.). (**g**) CGNs, transfected with control vectors, RNF157 RNAi or RNF157 RNAi and the RNF157-Res plasmid together with the β-Gal expression plasmid, were analyzed as in **2c**. A total of 2171 neurons from four independent experiments were included in the analysis (ANOVA, $^{***}P<0.001$, mean +S.E.M.). (**h**) Hippocampal neurons, transfected at DIV2 with control vector, the RNF157 RNAi #3, the RNF157-Res plasmid, or both the RNF157 RNAi #3 and RNF157-Res plasmids, were analyzed at DIV7. A total of 1099 neurons from four independent experiments were included in the analysis (ANOVA, $^{***}P<0.001$, mean +S.E.M.). (**i**) CGNs, transfected with control vector, the RNF157 or RNF157 ΔRING expression plasmids together with the β-Gal plasmid, were exposed to serum and KCl withdrawal for 24 h before analysis as described in **2c**. A total 1383 neurons from four independent experiments were included in the analysis (ANOVA, $^{*}P<0.05$ $^{***}P<0.001$, mean +S.E.M.)

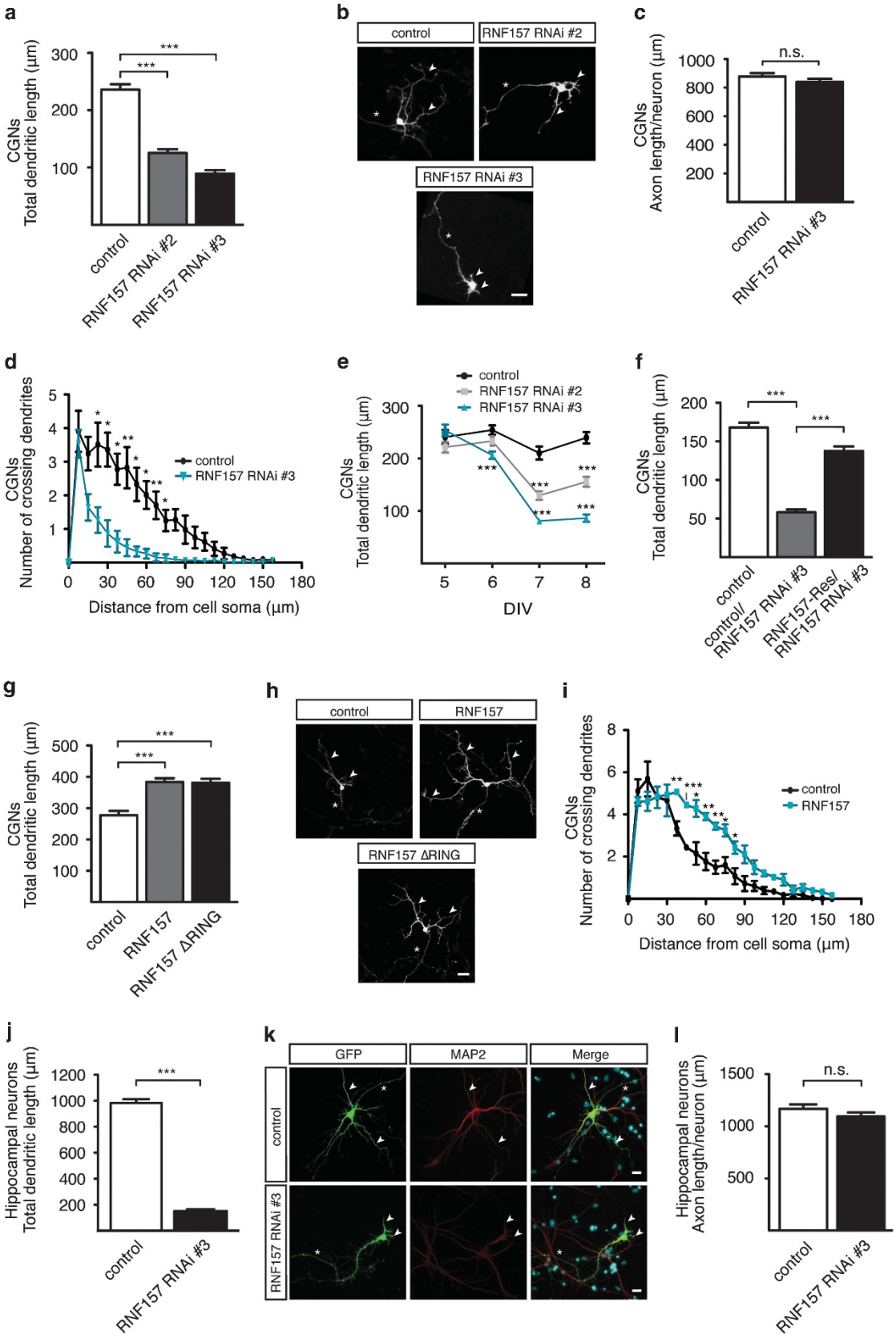

Figure 3 For caption see next page

Mapping analyses showed that RNF157 bound to the second PTB domain of Fe65 (Figure 4c) and Fe65 bound to an N-terminal region of RNF157 excluding the RING domain (Figure 4d). Owing to the highly homologous N-terminal region in MGRN1, we carried out co-immunoprecipitation analyses, which revealed that Fe65 also interacted with MGRN1 (Supplementary Figures S4d and e).

We also determined the expression pattern of Fe65 in cerebellum, cortex and hippocampus and found that Fe65 was abundantly expressed in these tissues and in cultured neurons (Figures 4e–g, Supplementary Figure S4f). At the subcellular level, Fe65 localized to the cytoplasmic and to the nuclear fraction (NF) of neurons (Figures 4h and i). Taken together, our experiments identify Fe65 as an interactor of RNF157 and demonstrate Fe65's cytoplasmic and nuclear localization in neurons.

The E3 ligase RNF157 ubiquitinates Fe65. Having identified Fe65 as an interaction partner of RNF157, we sought to determine whether Fe65 is a substrate of RNF157. First, we analyzed if RNF157 acts as an E3 ligase and tested the ability of wild-type RNF157 and ligase-dead RNF157 ΔRING to autoubiquitinate. We transfected HEK293T cells with RNF157 and RNF157 ΔRING, followed by immunoprecipitation from denatured lysates and immunoblotting for ubiquitin. Here, we found a clear autoubiquitination response of wild-type but not RNF157 ΔRING (Figure 5a). We next determined if RNF157 ubiquitinates Fe65 and if the ubiquitination is dependent on RNF157's ligase activity. In addition, we analyzed which type of ubiquitin chain was transferred. We expressed Fe65 together with RNF157 or RNF157 ΔRING and HA-tagged wild-type ubiquitin or ubiquitin mutants that fail to support lysine (K) 48 or K63-linkage ubiquitin chains. Polyubiquitin chains that utilize K48 typically trigger proteasomal degradation, while K63 chains are predominantly associated with non-proteasomal events, although exceptions have been reported.[21–24] The results showed that wild-type but not ligase-dead RNF157 stimulated the ubiquitination of Fe65 (Figures 5b and c) and that the ubiquitin K63R mutant abrogated ubiquitination of Fe65 (Figures 5b and c).

We then examined if Fe65 undergoes proteasome-dependent degradation. We exposed CGNs to proteasome inhibition and found a significant accumulation of Fe65, whereas 14-3-3 remained unaffected (Figure 5d). To test if ubiquitination of Fe65 may lead to either proteasomal or lysosomal degradation, we examined if the sensitivity to the deubiquitination inhibitor N-ethylmaleimide (NEM) changes the distribution of Fe65 in the cell. We used cortical lysates in the presence or absence of NEM and subjected them to a differential fractionation protocol. We used the Lamp1 and PSMA2 antibodies to track the lysosomes and the proteasomes, respectively. Here we found that in the presence of NEM, Fe65 accumulated to a greater extent in the pellet fractions where we found proteasomes but no lysosomes (Figure 5e).

To further determine the consequence of loss of RNF157 on Fe65 protein levels, we examined brain tissues isolated from P5 and 6-week-old wild-type and RNF157 $-/-$ mice. Although we found no significant difference in Fe65 protein levels at P5 (Figure 5f), we detected higher protein levels in 6-week-old mice in both cortical (Figure 5g) and hippocampal tissue (Supplementary Figures S5a and b). Importantly, we did not find a change in *Fe65* mRNA levels in the postnatal or adult mouse brain (Supplementary Figure S5c). Interestingly, we found an increase of Fe65 in both PNS and NFs in the 6-week-old cortices from RNF157 $-/-$ mice (Figure 5h). Although the PNS fractions appeared to contain Fe65 and its phosphorylated species, nuclear Fe65 appeared mostly unphosphorylated. We carried out additional Fe65 antibody/antigen competition experiments to verify the specificity of these bands (Supplementary Figure S5d). Taken together, these experiments suggested that Fe65 is ubiquitinated by RNF157 using K63-polyubiquitin chains and that the loss of RNF157 leads to a slow accumulation of Fe65 in the brain.

Fe65 regulates neuronal survival but not dendritic growth downstream of RNF157. To establish the role of the RNF157/Fe65 interaction in dendrite growth or in neuronal survival, we explored the function of Fe65 in neurons. We first generated different Fe65 RNAi plasmids and identified the effective Fe65 RNAi #3 (Figure 6a). Having confirmed the endogenous knockdown of Fe65 in neurons (Figure 6b), we examined whether Fe65 affects dendrites in CGNs, but found no indication that Fe65 knockdown alters dendritic growth (Figures 6c and d). We then tested if Fe65 has a role in neuronal survival. We exposed control-transfected neurons

Figure 3 RNF157 supports dendrite growth and maintenance. (**a**) CGNs, transfected at DIV4 with control vector, RNF157 RNAi #2 or #3 plasmids together with the Bcl-XL and GFP expression plasmids, were subjected to immunocytochemistry with the GFP antibody at DIV8, followed by morphological analyses. A total of 653 neurons from five independent experiments were analyzed (ANOVA, $^{***}P<0.001$, mean +S.E.M.). (**b**) Representative neurons from **3a**. Arrowheads and asterisks indicate dendrites and axons, respectively. Scale bar equals 20 μm. (**c**) Total axonal length measured in neurons from **3a**. (Student's *t*-test, NS, nonsignificant, mean +S.E.M.). (**d**) CGNs from **3a** were subjected to Sholl analysis, in which concentric circles are drawn around the cell soma of the neurons and the crossings of dendrites and circles are counted. A total of 89 neurons from three independent experiments were analyzed (Student's *t*-test, $^{*}P<0.05$, $^{**}P<0.01$, mean +S.E.M.). (**e**) CGNs, transfected at DIV4 with control vector, RNF157 RNAi #2 or #3 plasmids together with the Bcl-XL and GFP expression plasmids, were subjected to morphological analyses to measure dendrite length at DIV5, 6, 7 and 8. At total of 1550 neurons from four independent experiments were analyzed (ANOVA, $^{***}P<0.001$, mean +S.E.M.). (**f**) CGNs, transfected at DIV4 with control vectors, RNF157 RNAi #3 or RNF157 RNAi #3 together with the RNF157-Res plasmid, were subjected to morphological analyses at DIV8. A total of 322 neurons from three independent experiments were analyzed (ANOVA, $^{***}P<0.001$, mean +S.E.M.). (**g**) CGNs, transfected at DIV4 with control vector, the RNF157 or RNF157 ΔRING plasmids, were subjected morphological analyses at DIV8. A total of 315 neurons from three independent experiments were analyzed (ANOVA, $^{***}P<0.001$, mean +S.E.M.). (**h**) Representative images of neurons in **3g**. Arrowheads and asterisks indicate dendrites and axons, respectively. Scale bar equals 20 μm. (**i**) CGNs from **3g** were subjected to Sholl analysis. A total of 84 neurons from three independent experiments were analyzed (Student's *t*-test, $^{*}P<0.05$, $^{**}P<0.01$, $^{***}P<0.001$, mean +S.E.M.). (**j**) Hippocampal neurons, transfected at DIV4 with the control vector or RNF157 RNAi #3 plasmid were subjected to morphological analysis at DIV8. A total of 189 neurons from three independent experiments were included in the analysis (Student's *t*-test, $^{***}P<0.001$). (**k**) Representative images of hippocampal neurons in **3j** immunostained with the GFP and MAP2 antibodies. Arrowheads and asterisks indicate dendrites and axons, respectively. Scale bar equals 20 μm. (**l**) Measurement of longest process length (axons) of neurons in **3j**. A total of 189 neurons from three experiments were included in the analysis (Student's *t*-test, NS, nonsignificant, mean +S.E.M.)

and Fe65 RNAi neurons, without co-transfection of Bcl-XL, to serum/KCl withdrawal and determined the apoptotic rate induced by stress. Interestingly, we found that knockdown of Fe65 had a rescue-like effect in neurons (Figures 6e and f). To support this finding, we overexpressed Fe65 and found that this led to an increase in apoptosis (Figure 6g). Using a validated Fe65-Rescue (Res) plasmid (Figures 6h and i), we carried out a rescue experiment, in which we overexpressed wild-type Fe65 or Fe65-Res in the background of Fe65 RNAi. Although expression of wild-type Fe65/Fe65 RNAi had no effect on neuronal survival, expression of Fe65-Res/Fe65 RNAi led to a significant increase in cell death (Figure 6j).

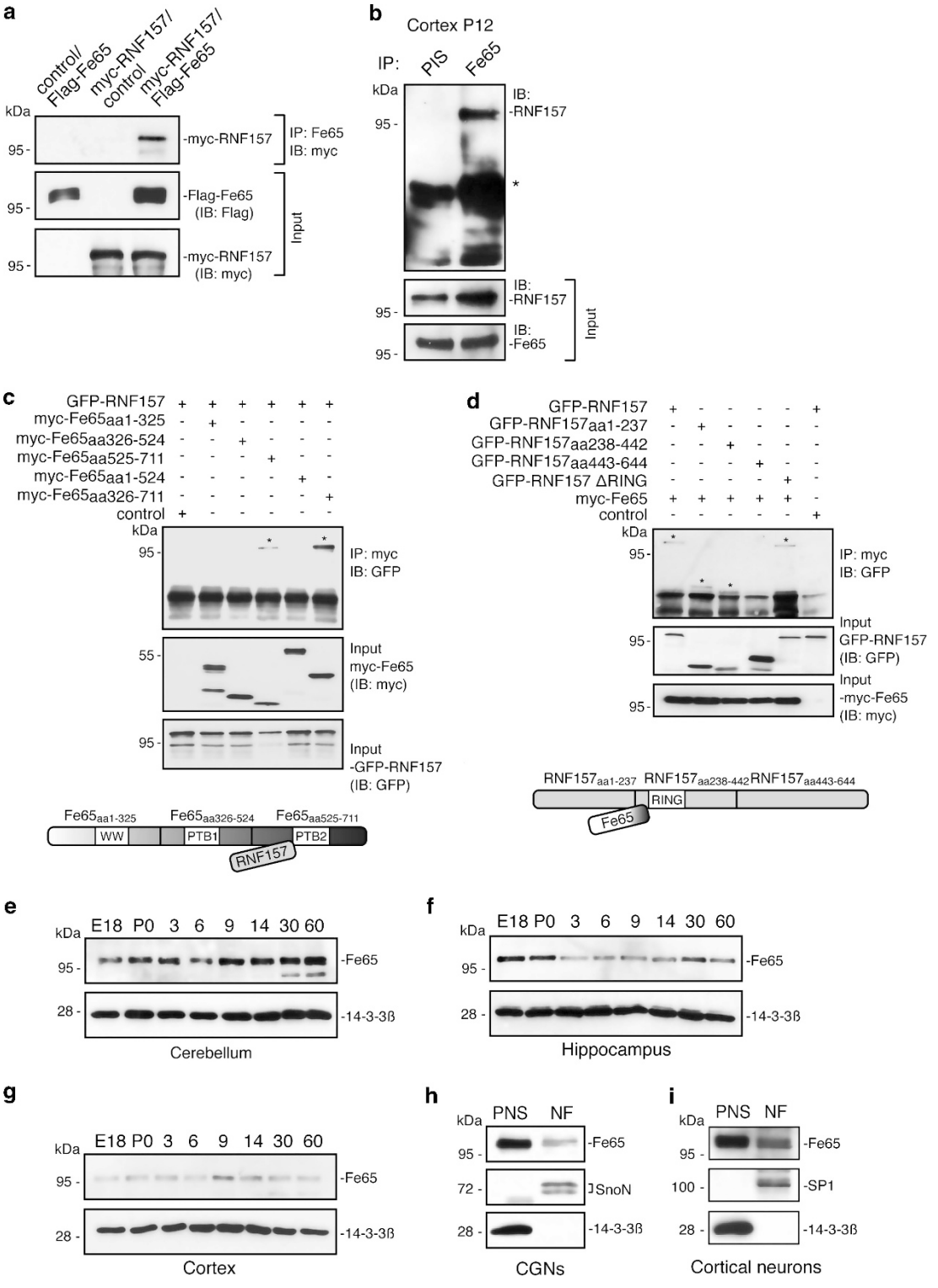

Figure 4 For caption see next page

These results established a role for Fe65 in neuronal apoptosis.

Finally, we determined the hierarchy between RNF157 and Fe65 in neuronal survival and carried out epistasis analyses in both CGNs and hippocampal neurons. We found that while knockdown of RNF157 increased the apoptosis rate, RNF157 and Fe65 double knockdown reversed this phenotype and restored the survival rate to control levels (Figures 6k–m), suggesting that, in the control of neuronal survival, Fe65 acts downstream of RNF157.

Nuclear Fe65 is particularly potent in inducing neuronal apoptosis. Owing to the presence of Fe65 in the cytoplasm and in the nucleus of neurons, we examined which localization of Fe65 is responsible for triggering apoptosis. We generated Fe65 mutants, which are targeted to the cytoplasm NES (nuclear exclusion sequence)-Fe65 or to the nucleus NLS (nuclear localization sequence)-Fe65. Strikingly, we found that expression of NLS-Fe65 but not NES-Fe65-induced apoptosis in CGNs (Figures 7a and b). We then examined Fe65 in structure function analyses for which we generated deletion mutants of Fe65 including Fe65-WW, Fe65-PTB1, Fe65-PTB2, Fe65-WW/PTB1 and Fe65-PTB1/PTB2 (Figure 7c). Of those, we found that Fe65-PTB2 translocated into the nucleus in neurons and in HEK293T cells (Figure 7d, Supplementary Figure S6). When expressed in CGNs, we observed that the Fe65-PTB2 mutant was very potent in inducing cell death, whereas all other mutants had little or no effect (Figure 7e). Similar analyses in hippocampal neurons revealed that expression of wild-type Fe65 and NLS-Fe65 were equally potent in inducing cell death (Figure 7f). Hippocampal neurons, however, appeared to be more sensitive to the overexpression of NES-Fe65 as it also triggered a significant increase in apoptosis (Figure 7f). These results suggest that the localization of Fe65 in the nucleus holds the potential to induce neuronal apoptosis.

Fe65 and Tip110 regulate neuronal survival in the nucleus. The strong induction of neuronal apoptosis by nuclear Fe65 raised the question of how nuclear Fe65 promotes neuronal cell death. A complex consisting of Fe65, the histone acetyl transferase Tip60 and APP-AICD (APP intracellular domain) has previously been shown to translocate into the nucleus to regulate gene transcription.[25] As Fe65 interacted robustly with Tip60 (Supplementary Figure S7a), we investigated if Tip60 has a role in neuronal apoptosis and overexpressed it in CGNs. The results, however, did not lead to the conclusion that Tip60 promoted apoptosis (Figure 8a). With another yeast two-hybrid screen to identify other nuclear interactors of Fe65, we found the nuclear RNA-binding protein Tip110 (or SART3) as a potential binding partner of Fe65. Tip110 has been identified as an HIV-1 Tat-interacting protein,[26] has a role in stem cells,[27,28] hematopoiesis[29] and gene transcription and expression,[26,30,31] but had not been implicated in any neuronal function. We first established the interaction of Fe65 and Tip110 in heterologous cells (Figure 8b), which was unaffected by the presence of RNF157 (Supplementary Figure S7b). Although we could not confirm the suitability of commercial Tip110 antibodies to determine a Tip110 expression profile, data from ALLEN Brain Atlas indicated a high expression level of Tip110 in the hippocampus and cortex. We also found that exogenous Tip110 localized to the nucleus in neurons (Figure 8c), which is consistent with a previous report that showed nuclear Tip110 in tumor cells.[32] In contrast to Tip60, overexpression of Tip110 strongly induced cell death in cultured neurons (Figures 8d–f), implicating Tip110 in neuronal apoptosis.

To examine if the Fe65-induced neuronal cell death is dependent on Tip110, we overexpressed Fe65, expressed the Tip110 RNAi plasmid (Figure 8g) or overexpressed Fe65 together with Tip110 RNAi in neurons. Interestingly, we found that Fe65-induced apoptosis was neutralized upon Tip110 knockdown, whereas Tip110 RNAi on its own had no effect (Figures 8h and i). Finally, we examined if Tip110 knockdown also ameliorates the induction of apoptosis in RNF157 RNAi neurons and found that Tip110 RNAi induced a partial rescue upon RNF157 knockdown (Figure 8j). Taken together, these findings suggest that the interaction of Fe65 and Tip110 in the nucleus is required to induce neuronal apoptosis.

Discussion

Neuronal health and the proper regulation of apoptosis are crucial for the long-term integrity of a neuronal network. In this study, we characterized a novel RNF157/Fe65/Tip110 pathway, which controls neuronal survival. The E3 ubiquitin ligases RNF157 and MGRN1 are homologous proteins in mammals, while the *Drosophila* genome harbors only one gene encoding CG9941. Both RNF157 and CG9941 display a nervous system-dominant expression with no detectable protein in non-neural tissue. Interestingly, a destabilizing mutation in the *Mgrn1* gene, which is strongly expressed in brain, leads to spongiform degeneration in the aged brain,[15] identifying MGRN-1 as a critical protein for the long-term integrity of the brain. In our study, we established a pro-survival function of

Figure 4 RNF157 interacts with the adaptor protein Fe65. (**a**) Lysates of HEK293T cells, transfected with control vector together with the Flag-Fe65 or the myc-RNF157 expression plasmids or the Flag-Fe65 and the myc-RNF157 expression plasmids, were subjected to immunoprecipitation with the Fe65 antibody followed by immunoblotting with the myc antibody. IP, immunoprecipitation; IB, immunoblotting. (**b**) Lysates of P12 mouse cortex, were subjected to immunoprecipitation with the Fe65 antibody or preimmune serum (PIS), followed by immunoblotting with the RNF157 antibody. Asterisk indicates Ig_H chains. (**c**) Lysates of HEK293T cells, transfected with plasmids encoding indicated Fe65 mutants together with the GFP-RNF157 plasmid, were subjected to immunoprecipitation with the myc antibody, followed by immunoblotting with the GFP antibody. Schematic representation of domain structure of Fe65 and Fe65 fragments. WW (tryptophan) domain, PTB (phospho tyrosine binding) domains and mapped RNF157 binding region. (**d**) Lysates of HEK293T cells, transfected with plasmids encoding GFP-RNF157 (wild type) or indicated RNF157 mutants together with the myc-Fe65 plasmid, were subjected to immunoprecipitation with the myc antibody, followed by immunoblotting with the GFP antibody. Schematic representation of domain structure of RNF157 and RNF157 fragments. RING domain and mapped Fe65 binding region. (**e, f** and **g**) Lysates of mouse cerebella, hippocampi and cortices isolated from E18, P0, P3, P6, P9, P14, P30 and P60 rats were immunoblotted with the Fe65 or 14-3-3β antibodies. The latter served as loading control. (**h** and **i**) CGNs and cortical neurons were subjected to subcellular fractionation, followed by immunoblotting with the Fe65 antibody. SnoN and SP1 served as quality control markers of NF and 14-3-3β of the PNS

RNF157 in neurons because acute RNF157 knockdown induced an apoptosis in different neuronal cell types. Taken together, our data and the study by He *et al.*[15] suggest that the related E3 ligases RNF157 and MGRN1 ensure neuronal health and integrity.

Our results show that RNF157 has a dual role in neurons as it is also required for dendrite growth and maintenance for which its ligase activity is not critical. We can only speculate that RNF157 may act as a scaffold molecule to regulate this process. RNF157's ligase activity, however, is required to

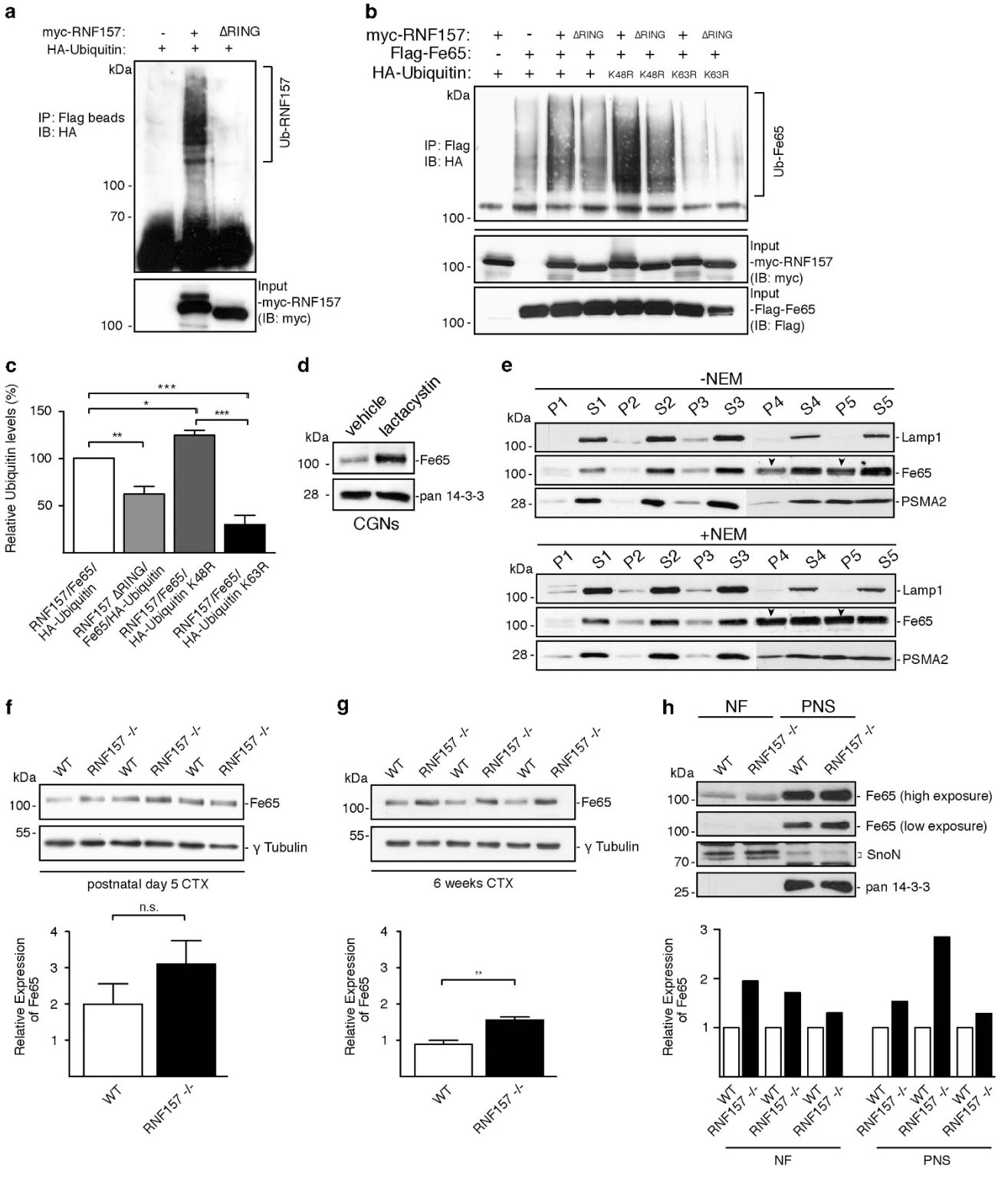

Figure 5 For caption see next page

support neuronal survival. With the adaptor protein Fe65, which has gained prominence owing to its interaction with amyloid precursor protein (APP) and its effect on APP processing,[19,20,33,34] we identified an interactor and substrate of RNF157 that has a pro-apoptotic gain-of-function. Despite the exclusive expression of Fe65 in the brain, deletion of the *Fe65* gene has no further consequences,[35] which is consistent with our finding that Fe65 RNAi has no effect on neuronal survival.

Our Fe65 loss-of-function analysis also did not reveal any effect on dendrite growth. A recent study, however, reported that expression of Fe65 leads to an increase in neurite length, the accompanying loss-of-function experiments consequently showed a decrease.[36] Although there appears to be an obvious discrepancy as to whether or not Fe65 controls neuronal morphology, it can be attributed to the differences in the experimental design. Hence, it would require further experiments if Fe65 loss-of-function critically affects the initiation of neurites but not so much already established axons and dendrites.

Our results support the view that ubiquitination of Fe65 by RNF157 leads to formation of K63-polyubiquitin chains rather than K48-linked chains. The consequence of this type of ubiquitination is typically associated with functional modification or stabilization,[21–23] but degradation by the proteasome has also been reported.[24] In the light of our findings that Fe65 is epistatic to RNF157 in axon growth control, proteasomal inhibition leads to accumulation of Fe65 and that Fe65 co-migrates with proteasomal components, together with the accumulation of Fe65 protein in the brain of the RNF157 −/− mouse, ubiquitination of Fe65 likely leads to proteasomal degradation.

Although RNF157 and MGRN1 share sequence similarities, it seems unlikely that there is complete functional redundancy as the MGRN1 mutant mouse shows age-dependent neurodegeneration,[15] for which RNF157 probably cannot compensate. We found that the RNF157 knockout mouse is also viable, suggesting that these ligases fully compensate for each other at least during development. As we found that Fe65 also associates with MGRN1, both RNF157 and MGRN1 may act on Fe65 in a compensatory manner. Our cell culture system, however, which induces acute loss of RNF157 as opposed to systemic loss of RNF157 in the mouse, revealed a role in neuronal survival, which may become relevant in the aged brain.

Our experiments showed that in particular nuclear Fe65 acts as a regulator of neuronal apoptosis. A previous report identified the nuclear complex Fe65/Tip60/APP.[25] Although our experiments do not support a role for Tip60 in apoptosis, our results suggest that Fe65 acts together with the RNA-binding protein Tip110 in the control of apoptosis. According to the ALLEN Brain Atlas, Tip110 appears to be highly expressed in the nervous system, and with this study, we introduce Tip110 as a novel pro-apoptotic protein in neurons.

Although RNF157 lies upstream of Fe65 and Tip110 in the control of neuronal survival, RNF157 appears to have a different role in *Drosophila*. In contrast to CG9941, Fe65 is not conserved in the fly but an invention of higher ordered species of the animal kingdom. This may also explain why we do not observe neuronal cell death in the fly brain. Collectively, our data indicate that while evolutionarily conserved, the E3 ligase RNF157 may have a different function in the fly, whereas in mammalian neurons it regulates dendrite growth and neuronal survival.

Materials and Methods

Plasmids. Rat *Rnf157* was amplified from cerebellar granule neuron cDNA and cloned into pCMVmyc or pEGFP-C2 to produce a myc- or GFP-tagged RNF157 protein. RNF157 ΔRING was created by subcloning the fusion PCR product of RNF157, which lacks the RING domain, into the pCMVmyc plasmid. pcDNA3.1-myc-Fe65 was a gift from Uwe Konitzko (University of Zurich, Zurich, Switzerland), Flag-Fe65 was a gift from Toshiharu Suzuki (University of Hokkaido, Hokkaido, Japan). In addition, Fe65 was subcloned into the pCMVmyc plasmid. pBICEP-cmv-Tip60 was a gift from Gregor Eichele (MPI of Biophysical Chemistry, Göttingen, Germany). pCS2-HA-hTip110 and pCS2-myc-hTIP110 were gifts from Michael Rape (University of California, Berkeley, CA, USA). pEGFP-C1-mMGRN1 was gift from Ramanujan Hedge (Cambridge Biomedical Campus, Cambridge, UK).

The shRNA plasmids were generated by cloning of the following RNAi targeting regions into a modified pBluescript-U6 plasmid: RNF157 RNAi #2: 5′-AGAGGAC ATGCGCATTTCTA-3′; RNF157 RNAi #3: 5′-GGACAATAAGCTGTGCTCTG-3′; Fe65 RNAi #3: 5′-AAGCTGACCCAGATGCTCAA-3′; Tip110 RNAi 5′-AGTCAGTACCTAG ATCGACA-3′.

Site-directed mutagenesis of the RNF157 and Fe65 targeting regions was performed using standard protocols and confirmed by sequencing. The myc-NES-Fe65 and myc-NLS-Fe65 plasmids were constructed by appending the Fe65 sequence with the HIV-1 *Rev* NES and SV40 large T-antigen NLS, respectively.

Antibodies. The antibodies used in this study include rabbit anti-RNF157 (Sigma Aldrich, Hamburg, Germany), mouse anti-pan14-3-3 or anti-14-3-3β (Santa Cruz, Heidelberg, Germany), rabbit anti-SP1 (Santa Cruz), mouse anti-N-Cadherin (Becton Dickinson, Heidelberg, Germany), mouse anti-myc (Santa Cruz), mouse anti-β-galactosidase (Santa Cruz), rabbit anti-cleaved caspase-3 (Cell Signaling, Danvers, MA, USA), rabbit anti-GFP (Invitrogen/Life Technologies, Darmstadt,

Figure 5 RNF157 ubiquitinates the adaptor protein Fe65. (**a**) Lysates of HEK293T cells, transfected with the myc-RNF157 or the myc-RNF157 ΔRING plasmid together with the HA-ubiquitin expression plasmid, were subjected to a denaturing protocol followed by immunoprecipitation with the myc antibody and immunoblotting with the HA-antibody. (**b**) Lysates of HEK293T cells, transfected with the myc-RNF157 or the myc-RNF157 ΔRING plasmid and the Flag-Fe65 plasmid together with plasmids encoding HA-ubiquitin WT or indicated ubiquitin mutants, were subjected to a denaturing protocol followed by immunoprecipitation with Flag-sepharose beads and immunoblotting with the HA-antibody. (**c**) Quantification of three independent experiments of which one is depicted in **4b** (ANOVA, $*P<0.05$, $**P<0.01$, $***<0.001$, mean +S.E.M.). (**d**) CGNs (DIV2) were exposed to lactacystin for 5 h. Lysates were then analyzed using immunoblotting with the Fe65 or 14-3-3β antibodies. The latter served as loading control. (**e**) Lysates from mouse cortices (8 weeks), in the presence and absence of NEM, were subjected to differential centrifugation procedure, in which the lysate was first centrifuged at 2000 *g*, and then divided into supernatant 1 and pellet 1. Supernatant 1 was then subjected to a run at 4000 *g* and again divided into supernatant 2 and pellet 2. This procedure was repeated at 10 000 *g*, 100 000 *g* and 335 000 *g*. Indicated pellets 1–5 and supernatant fractions 1–5 were immunoblotted with the lysosomal marker Lamp1, the proteasomal marker PSMA2 and Fe65. Arrowheads indicate enrichment of Fe65. (**f** and **g**) Cortical lysates from P5 (**f**) and 6 weeks old (**g**) wild-type and RNF157 −/− littermates (three pairs) were immunoblotted with the Fe65 and γ–tubulin antibodies. The latter served as loading control. Graphs show quantification of blots. Three independent littermates were included in the analyses (Student's *t*-test, $**P<0.01$, NS, nonsignificant). (**h**) Week 6 wild-type and RNF157 −/− cortices were subjected to subcellular fractionation followed by immunoblotting with the Fe65, SnoN and pan14-3-3 antibodies. The latter two served as quality control for NF and PNS, respectively. Graphs show quantification of relative expression of Fe65 in the NF and PNS fractions from three independent littermates

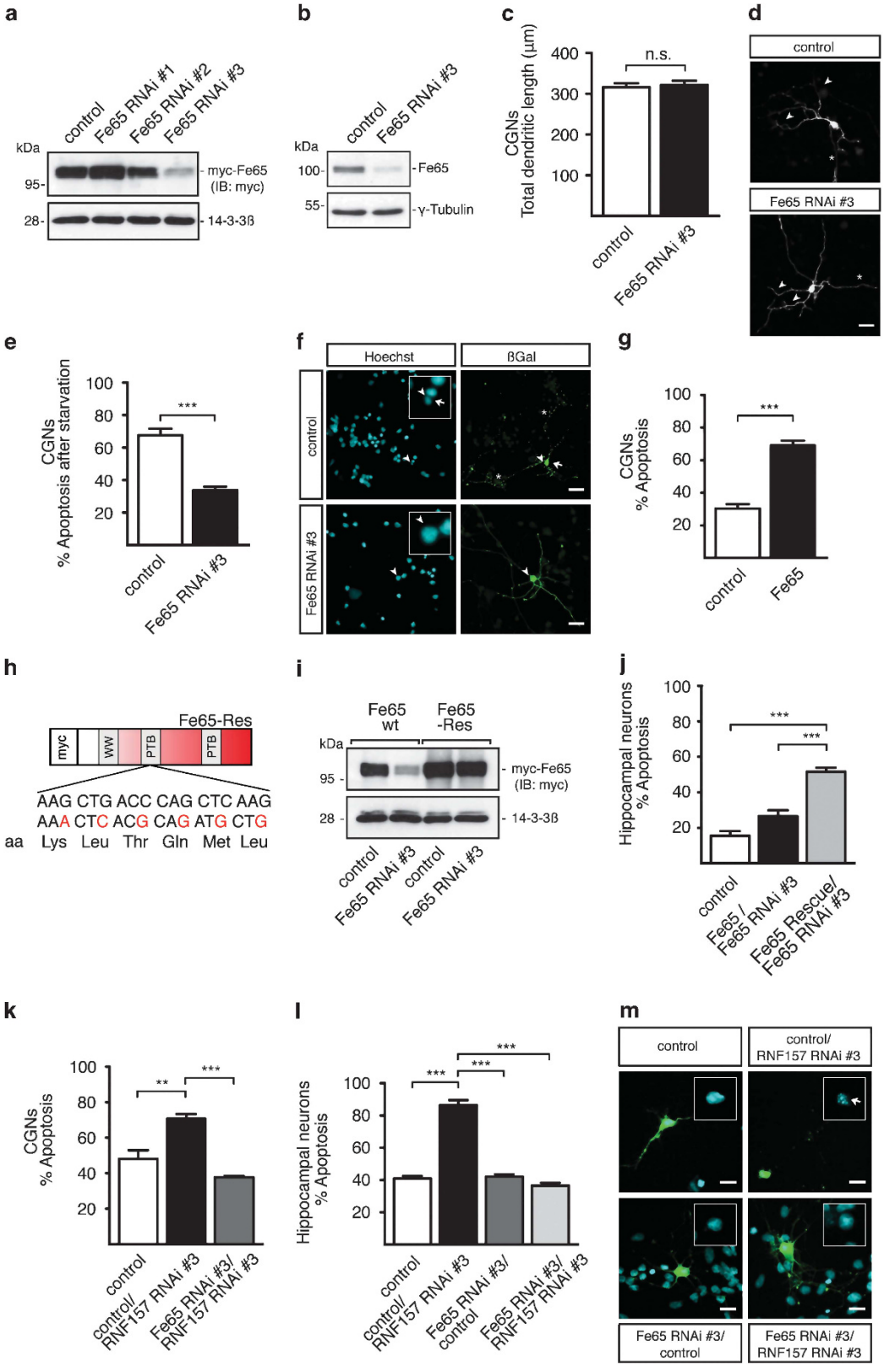

Figure 6 For caption see next page

Germany), mouse anti-GFP (Santa Cruz), rabbit anti-Fe65 (Santa Cruz), mouse anti-Flag (Sigma Aldrich), M2 Flag affinity beads (Sigma Aldrich), mouse anti-HA (Santa Cruz), rabbit anti-HA (Abcam, Cambridge, UK), mouse anti-γ-tubulin (Sigma Aldrich), rabbit anti-LAMP1 (Santa Cruz) and rabbit anti-PSMA2 (Cell Signaling).

Yeast two-hybrid. The identification of RNF157 interaction partners was performed according to the Matchmaker Gold Yeast Two-Hybrid protocol using the N-terminal fragment of RNF157 (bp 1–971) including the RING domain and the C-terminal fragment of Fe65 (bp 978–2133) including the phospho tyrosine-binding domains as bait, cloned into the pGBT9 Gal4-binding vector (Clontech, Mountain View, CA, USA). As prey, a Mate & Plate Human Fetal Brain library was utilized.

RNF157 gene trap mouse. ES cells that carry a mutant allele were purchased from Texas A&M Institute for Genomic Medicine (TIGM, College Station, TX, USA). The mouse *Rnf157* gene is located on chromosome 11 and consists of 19 exons. The gene trap cassette harboring a β-*Geomycin* gene was inserted into intron 2, which can be detected with specific primers. ES cells were injected into FVB/N blastocysts to generate chimeric mice. Chimera were mated with C57B/6 and screened for germline transmission. Animals were housed under a standard 12-h light–dark cycle with food and water *ad libitum* in the animal facility of Max Planck Institute of Experimental Medicine, Göttingen, Germany.

X-Gal staining. Forty micrometer sagittal sections of RNF157+/+ and RNF157 $-/-$ brains were cut using a vibratome (Leica VT1000S, Wetzlar, Germany) and incubated overnight at 37 °C in X-Gal solution (2 mM $MgCl_2$, 0.02% NP40, 0.01% sodium deoxycholate, 5 mM potassium ferrocyanide, 5 mM potassium ferricyanide and 0.5 mg/ml X-gal in PBS) under lightproof conditions. Following several washes in PBS, the sections were collected and dried on microscope slides before imaging.

Immunoprecipitation, subcellular fractionation and immunoblotting. For co-immunoprecipitation, transfected HEK293T cells or the respective murine brain tissues were lysed in buffer containing 1% NP40, 150 mM NaCl, 20 mM Tris, pH 7.4, 1 mM EDTA, 10% glycerol supplemented with protease inhibitors Aprotinin (3 μg/ml), Leuptin (1 μg/ml), Pepstatin (1 μg/ml) and DTT (1 mM). Lysates (1 mg) were incubated with the primary antibody for 4 h or overnight at 4 °C, followed by precipitation of the protein–antibody complex using protein A-sepharose beads (GE Healthcare, Little Chalfont, UK) for 45 min. The protein-bound beads were washed several times in Triton X-100 buffer (150 mM NaCl, 50 mM Tris-HCl, pH 7.5, 1 mM EDTA, 1% Triton X-100) followed by PBS and eluted by boiling the beads in SDS sample buffer.

For subcellular fractionation, cultured neurons or cortices were lysed in detergent-free buffer A (10 mM HEPES, pH 7.9, 10 mM KCl, 0.1 mM EGTA, 0.1 mM EDTA, protease inhibitors) and subjected to mechanic disruption using a 2 ml dounce. Nuclei were spun down for 5 min at 2000 r.p.m. at 4 °C and supernatant was used as PNS I. Nuclei were washed several times in buffer A supplemented with 0.1% NP40 and spun down at 380 g, followed by lysis in buffer B (20 mM HEPES, pH 7.9, 400 mM NaCl, 1 mM EDTA, 1 mM EGTA, protease inhibitors). Nuclei were extracted for 20 min at 4 °C and pelleted by centrifugation at 18 500 *g* for 20 min at 4 °C. Supernatant was harvested as NF. For further fractionation, the PNS I was ultracentrifuged for 40 min at 4 °C at 21 000*g*, the resulting pellet I and PNS II were harvested. PNS II was then ultracentrifuged for 2.5 h at 4 °C at 2 57 000 *g* resulting in pellet II and the cytoplasmic fraction.

Rat and mouse tissue samples at different embryonic or postnatal stages and lysates of neurons at various DIV were lysed in Triton X-100 buffer (150 mM NaCl, 50 mM Tris-HCl, 1 mM EDTA, 1% Triton X-100) supplemented with protease inhibitors, boiled in SDS sample buffer and analyzed by SDS-PAGE and subsequent immunoblotting analysis as previously described.

Ubiquitination assay. To avoid detection of nonspecific ubiquitination, ubiquitination assays were performed under denaturing conditions according to the protocol of Lu *et al*.[37] with some modifications. Briefly, transfected HEK293T cells were lysed in RIPA buffer without SDS (50 mM Tris-HCl, pH 8.0, 150 mM NaCl, 1% NP40, 0.5% sodium deoxycholate, 5 mM EDTA, protease inhibitors and 10 mM NEM). Then, 1 mg of total protein was incubated in 1% SDS for 5 min at 4 °C, boiled for 12.5 min at 95 °C, diluted 10x in lysis buffer (50 mM HEPES, pH 7.5, 150 mM NaCl, 10% glycerol, 1.5 mM $MgCl_2$, 1% Triton X-100) to adjust the concentration of SDS to 0.1% and immunoprecipitated with an antibody or with antibody-conjugated beads overnight at 4 °C. For non-conjugated antibodies, the antibody–antigen complex was immunoprecipitated for 45 min at 4 °C using Protein A-Sepharose. Precipitated proteins (on beads) were washed twice with lysis buffer, twice with HNTG buffer (20 mM HEPES, pH 7.5, 150 mM NaCl, 0.1% Triton X-100, 10% glycerol) and eluted by boiling the beads in SDS sample buffer. Lysates were analyzed by SDS-PAGE and subsequent immunoblotting analysis.

HEK293T cell culture and transfection. HEK293T cells were cultured in Dulbecco's modified Eagle's medium (DMEM) supplemented with 10% fetal calf serum (FCS) and 1% glutamine (GlutaMAX, Gibco/Life Technologies). Cells were transfected using the modified calcium phosphate method. Desired amount of DNA was diluted in sterile H_2O and mixed with 2.5 M $CaCl_2$ and 2xHBSS buffer (dissolve 4 g NaCl, 0.1775 g KCl, 0.095 g Na_2HPO_4 x $7H_2O$, 0.675 g glucose and 2.5 g HEPES in 250 ml ultrapure water and adjust pH to 7.05, 7.08 and 7.11). Precipitate was added to cultured HEK293T cells.

Primary neuron culture and transfection. CGNs were isolated at P6 from Wistar rats and transfected using a modified calcium phosphate method as described.[38] Hippocampal neurons were prepared from embryonic day (E) 18 rat embryos according to the protocol of Goslin *et al*.[39] with some modifications. Briefly, isolated hippocampi were incubated in 0.005% trypsin solution for 20 min followed by plating of the dissociated neurons on coverslips coated with poly-L-lysine at a density of 60 000 cells/cm^2 to 100 000 cells/cm^2 in DMEM

Figure 6 Fe65 promotes neuronal apoptosis but not dendrite growth. (**a**) Lysates of HEK293T cells, transfected with the myc-Fe65 plasmid together with control vector or different Fe65 RNAi constructs, were immunoblotted with the myc or 14-3-3β antibodies. The latter served as loading control. (**b**) Cortical neurons were mixed with control vector or Fe65 RNAi #3 plasmid and subjected to electroporation using the Amaxa nucleofector. After 5 days in culture, lysates of neurons were immunoblotted with the Fe65 or the γ-tubulin antibodies. The latter served as loading control. (**c**) CGNs, transfected at DIV4 with control vector or the Fe65 RNAi #3 plasmid together with the Bcl-XL and GFP expression plasmids, were subjected to morphological analyses at DIV8. A total of 217 neurons from three independent experiments were included in the analyses (Student's *t*-test, NS, nonsignificant, mean +S.E.M.). (**d**) Representative images of **6c**. Arrowheads and asterisks indicate dendrites and axons, respectively. Scale bar equals 20 μm. (**e**) CGNs were transfected at DIV2 with control plasmid or the Fe65 RNAi#3 plasmid together with the β-Gal plasmid, and exposed to serum and KCl withdrawal for 18 h before analysis as described in **2c**. A total of 1468 neurons from four independent experiments were included in the analysis (Student's *t*-test, $^{***}P<0.001$, mean +S.E.M.). (**f**) Representative images of transfected neurons from **6e**. Arrowheads indicate nuclei, while asterisks indicate apoptotic bodies and arrow indicates pyknotic nucleus. Scale bar equals 20 μm. (**g**) CGNs were transfected at DIV2 with control plasmid or the Fe65 expression plasmid together with the β-Gal plasmid and analyzed as described in **2c**. A total of 1037 neurons from three independent experiments were included in the analysis (Student's *t*-test, $^{***}P<0.001$, mean +S.E.M.). (**h**) Schematic representation of Fe65 domain structure and silent mutation in Fe65 RNAi targeting region. WW, WW domain; PTB, phospho tyrosine-binding domain. (**i**) Lysates of HEK293T cells, transfected with the myc-Fe65 wt or myc-Fe65-Res plasmids together with control vector or the Fe65 RNAi #3 plasmid, were immunoblotted with the myc and 14-3-3β antibodies. The latter served as loading control. (**j**) Hippocampal neurons, transfected at DIV2 with control vectors or Fe65 RNAi together with Fe65 WT or Fe65-Res expression plasmids, were analyzed as in **2c** at DIV6. A total of 1140 neurons from four independent experiments were included in the analysis (ANOVA, $^{***}P<0.001$, mean +S.E.M.). (**k**) CGNs, transfected at DIV2 with control vectors, the RNF157 RNAi #3 plasmid or both RNF157 RNAi #3 and Fe65 RNAi #3 constructs, were analyzed as in **2c** at DIV6. A total of 1765 neurons from three independent experiments were included in the analysis (ANOVA, $^{**}P<0.01$, $^{***}P<0.001$, mean +S.E.M.). (**l**) Hippocampal neurons, transfected at DIV2 with control vector, the RNF157 RNAi #3, the Fe65 RNAi #3, or both the RNF157 RNAi and Fe65 RNAi #3 plasmids together with the β-Gal construct, were analyzed as in **2c** at DIV6. A total of 1305 neurons from three independent experiments were included in the analysis (ANOVA, $^{***}P<0.001$, mean +S.E.M.). (**m**) Representative images of transfected neurons from **6l**. Insets depict nuclei of transfected neurons and arrow indicates pyknotic nucleus. Scale bar = 20 μm

supplemented with 10% FCS, 1% PSG (100 U/ml penicillin, 100 μg/ml streptomycin, 0.292 mg/ml L-glutamine) and 0.0125 mM glutamate. Twenty-four hours after plating, medium was exchanged with Neurobasal medium supplemented with 2% B27 (Life Technologies) and antibiotics. Neurons were transfected using a modified calcium phosphate method. Briefly, conditioned medium from neurons was collected and replaced by DMEM for 45 min to starve cells. DNA precipitates were added for 18 min before washes with DMEM and addition of the conditioned medium.

Survival assay in primary neurons. Cerebellar granule and hippocampal neurons were transfected at DIV2 with the indicated plasmids together with a β-galactosidase expression plasmid (0.3 μg) to visualize transfected neurons.

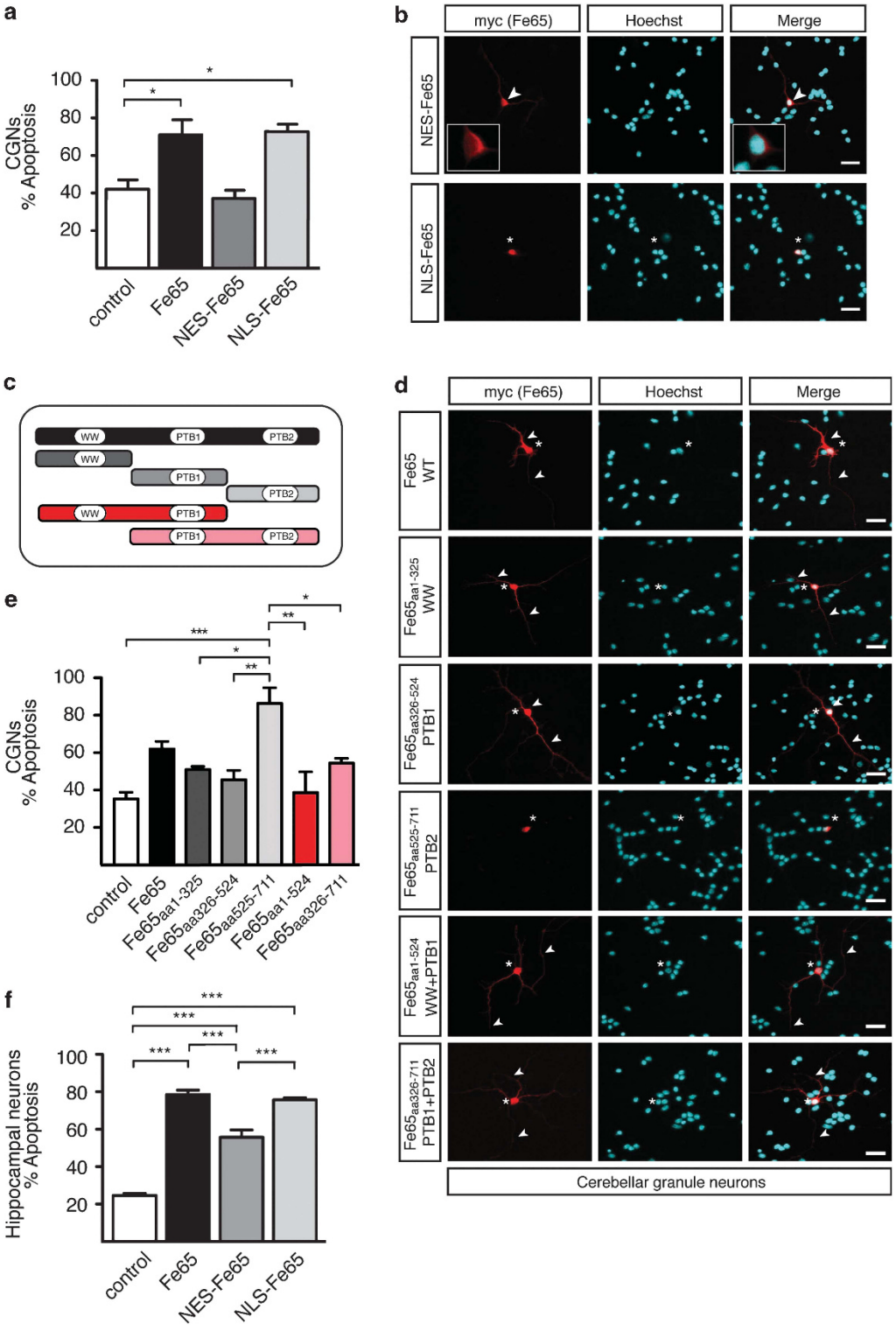

Figure 7 For caption see next page

To induce neuronal stress, cultures were deprived of conditioned medium and left in BME supplemented with insulin (10 μg/ml), glucose (35 mM) and 1% PSG for a certain amount of time depending on the experiment. Neurons were fixed with 4% paraformaldehyde after 4 or 5 DIV and subjected to indirect immunofluorescence using a β-galactosidase antibody. Cellular viability was assessed in β-galactosidase-expressing neurons based on the appearance of the neurites and the integrity of the nuclei, which were counterstained with the DNA dye DAPI (4′,6-diamidino-2-phenylindol) (Sigma-Aldrich). Survival assays were performed in a blinded manner. At least 100 neurons per condition were analyzed for statistical significance using GraphPad Prism 5.0 (GraphPad Software, La Jolla, CA, USA; ANOVA; Bonferroni´s *post hoc* test or Student's *t*-test).

Neuronal morphometry. For loss- and gain-of-function experiments, neurons were transfected with the respective expression plasmids together with an expression plasmid for GFP (0.3 μg) and the anti-apoptotic protein Bcl-XL (0.3 μg) because of possible effects of these manipulations on cell survival in a 24-well plate. The calcium phosphate precipitate was placed on granule neurons starved for 45 min for 15 min. After fixation with 4% PFA at the appropriate time points, neurons were subjected to immunocytochemistry using a polyclonal GFP antibody. Analysis of the morphology of axons and dendrites *in vitro* was carried out by capturing at least 30 random pictures of GFP-positive neurons in a blinded manner using a fluorescence microscope at x20 magnification. Axon and dendrite length was measured from the same granule neuron using ImageJ 1.410 software (http://rsb.info.nih.gov/ij).

Preparation of organotypic cortical slice cultures and transfection. Organotypic cortical slices were prepared from newborn (P0) C57BL/6 mice according to the Stoppini method with some modifications.[40] Briefly, animals were killed by decapitation, and the brain was quickly removed. Cortical hemispheres were isolated and 350 μm thick sagittal sections were cut with a McIlwain tissue chopper. The slices were separated and transferred to sterile, porous membrane units (0.4 μm; Millicell-CM, Millipore/Merck, Hessen, Germany), which were placed into six-well trays containing 1 ml of incubation medium (25% MEM without L-glutamine and HEPES, 25% BME without L-glutamine, 25% horse serum, 2.5% HEPES, 0.65% glucose and 1% PSG (100 μ/ml penicillin, 100 μg/ml streptomycin, 0.292 mg/ml L-glutamine). Cultures were kept at 37 °C in 5% CO_2 and fed every 2 days by 50% medium exchange. Cortical slice cultures were transfected at DIV2 using the transfection reagent Lipofectamine 2000. Briefly, plasmid DNA (2 μg pAAV-GFP-Synapsin and 10 μg control U6 or the RNF157 RNAi #1 or #3) or 10 μl Lipofectamine reagent were diluted in 250 μl Opti-MEM, mixed and incubated for 20 min at RT to allow complex formation. DNA-Lipofectamine mix was added carefully onto the slices and incubated for 1 h at 37 °C in 5% CO_2. Slices were washed with incubation media and 50% of the media was replaced.

Differential centrifugation. All procedures were carried out at 4 °C or on ice. Centrifugations at 100 000 *g* or higher were performed in a Beckman Optima XL80 ultracentrifuge (Beckman Coulter, Krefeld, Germany). Mouse cortical hemispheres were lysed in sucrose buffer (320 mM sucrose, 10 mM HEPES, pH 7.9, 1 mM EDTA, 1 mM EGTA, protease inhibitors, phosphatase inhibitors) supplemented with 10 mM NEM or vehicle and homogenized using 25 strokes in a 2 ml dounce. After 15 min on ice, the cell homogenate was centrifuged at 2000 *g* for 10 min. The supernatant was collected in a new tube and the pellet was washed twice with sucrose buffer followed by lysis in buffer B (20 mM HEPES, pH 7.9, 400 mM NaCl, 1 mM EDTA, 1 mM EGTA, protease inhibitors) and pelleted by centrifugation at 13 000 r.p.m. for 20 min at 4 °C. Supernatant was harvested as NF (P1). The previously collected supernatant and washes were combined into supernatant 1 (S1) and centrifuged at 4000 *g* for 10 min. The supernatant was collected in a new tube and the pellet (P2) washed twice with sucrose. The supernatant and washes were combined (S2) and centrifuged at 10 000 *g* for 12 min. The supernatant was collected in a new tube and the pellet (P3) washed twice with sucrose. The collected supernatant and washes (S3) were centrifuged at 100 000 *g* for 30 min and separated into pellet (P4) and supernatant (S4). Finally, the supernatant was centrifuged at 360 000 *g* and separated into pellet (P5) and supernatant (S5).

Quantitative PCR. For *Fe65* mRNA expression level in RNF157 transgenic mice, total RNA of wild-type and RNF157 $-/-$ cortices was isolated using the TRIZOL reagent (Invitrogen). cDNA was then synthesized using the SuperScript III First-Strand Synthesis System (Invitrogen). To amplify an Fe65 fragment, cDNA was mixed with the Power SYBR Green PCR Master Mix (Invitrogen) and the forward (5′-ATGCGAAACAGTGCAGCCAGTGATGA-3′) and reverse (5′-AGTAGTAGGTC CCTGAGGTGTCCT-3′) primers. Beta-actin primers were used as loading control.

Fly experiments

Flies: The CG9941-promoter was generated by cloning the putative regulatory region into the pPT-GAL plasmid. The primers 5′-CCTTCAAACCGTTGGCAA CGCTGG-3′ (located 569-bp upstream the starting ATG) and the primer 5′-CCGACTCCTTGCGAATGTTGACC-3′ (located 257-bp downstream the ATG) were used. The BestGene Inc. (Chino Hill, CA, USA) microinjected the plasmid into a w^{1118} background to generate the CG9941-GAL4 driver line.

Fly immunohistochemistry. Third instar larvae were dissected in PBS and then fixed in 4% PFA for 2 h. Then they were washed three times for 15 min in PBS 1%Tween20 and followed by incubation in blocking solution (1% BSA, 4% NGS in PBS 1%Tween20) for 2 h. Larvae were incubated overnight with the primary antibodies anti-GFP (GeneTex, Irvine, CA, USA – 1 : 500) and anti-nc82 (Developmental Studies *Hybridoma Bank*, Iowa City, IA, USA – 1 : 20), washed three times for 15 min with PBS 1%Tween20, incubated with the secondary antibodies Alexa Fluor 488 goat anti-chicken (1 : 300) and Alexa Fluor 633 goat anti-mouse (1 : 300) for 2 h, washed three times for 15 min with PBS 1%Tween20 and then mounted using DABCO (Roth, Karlsruhe, Germany).

Fly brains were removed from the head capsule in PBS and then fixed in 4% PFA for 1 h. Antibody staining followed the same procedure used for the larval preparation. Confocal microscopy was carried out using Leica TCS SP5 microscope.

Semiquantitative PCR. *CG9941* mRNA expression level was assessed in the knockdown flies by semiquantitative PCR. Total RNA of *upstream activating sequence-CG9941-RNAi*, *elav-GAL4* and elav-*CG9941-GAL4* was purified using the RNeasy Mini *Kit* (Qiagen, Valencia, CA, USA) and retro-transcribed to cDNA using the QuantiTect Reverse Transcription (Qiagen).

In each PCR reaction, a fragment of the constitutively expressed *spt6* mRNA (513 bp) and a portion of one *CG9941* mRNA (597) were amplified, using the following oligonucleotides: SPT6for 5′-GCGTCAAAGTCGAGAGACG-3′; SPT6rev 5′-GCCCAGATCCTCATCGTACT-3′; CG9941for 5′-CAGTATGTGGCCAGGGCT-3′; CG9941rev 5′-GTTCGTCGATAAAGCGCACC-3′.

Figure 7 Nuclear Fe65 triggers neuronal apoptosis. (**a**) CGNs were transfected at DIV2 with control plasmid, the Fe65, NES-Fe65 or NLS-Fe65 expression plasmid together with the β-Gal construct, and analyzed as described in **2c**. A total of 1834 neurons from three independent experiments were included in the analysis (ANOVA, $^*P<0.05$, mean +S.E.M.). (**b**) Representative images of **7a**. Arrowheads and asterisks indicate cytoplasmic and nuclear localization of Fe65, respectively. Inset displays higher magnification of NES-Fe65-transfected neuron. Scale bar = 20 μm. (**c**) Schematic representation of Fe65 deletion mutants (WW, WW domains; PTB, phospho tyrosine-binding domain). (**d**) CGNs, transfected at DIV2 with control vector, the myc-Fe65 construct or plasmids encoding indicated myc-Fe65 deletion mutants, were subjected to immunocytochemistry using the myc antibody and the DNA dye bisbenzimide. Asterisks and arrowheads indicate cell bodies and processes, respectively. Scale bar = 20 μm. (**e**) CGNs were transfected at DIV2 with control vector, the myc-Fe65 construct or plasmids encoding indicated Fe65 deletion mutants together with the β-Gal plasmid, and analyzed as in **2c** at DIV6. A total of 3203 neurons from three independent experiments were included in the analysis (ANOVA, $^*P<0.05$, $^{**}P<0.01$, $^{***}P<0.001$, mean +S.E.M.). (**f**) Hippocampal neurons were transfected at DIV2 with control plasmid, the myc-Fe65, NES-Fe65 or NLS-Fe65 expression plasmids together with the β-Gal plasmid, and analyzed at DIV6. A total of 1361 neurons from four independent experiments were included in the analysis (ANOVA, $^{***}P<0.001$, mean +S.E.M.)

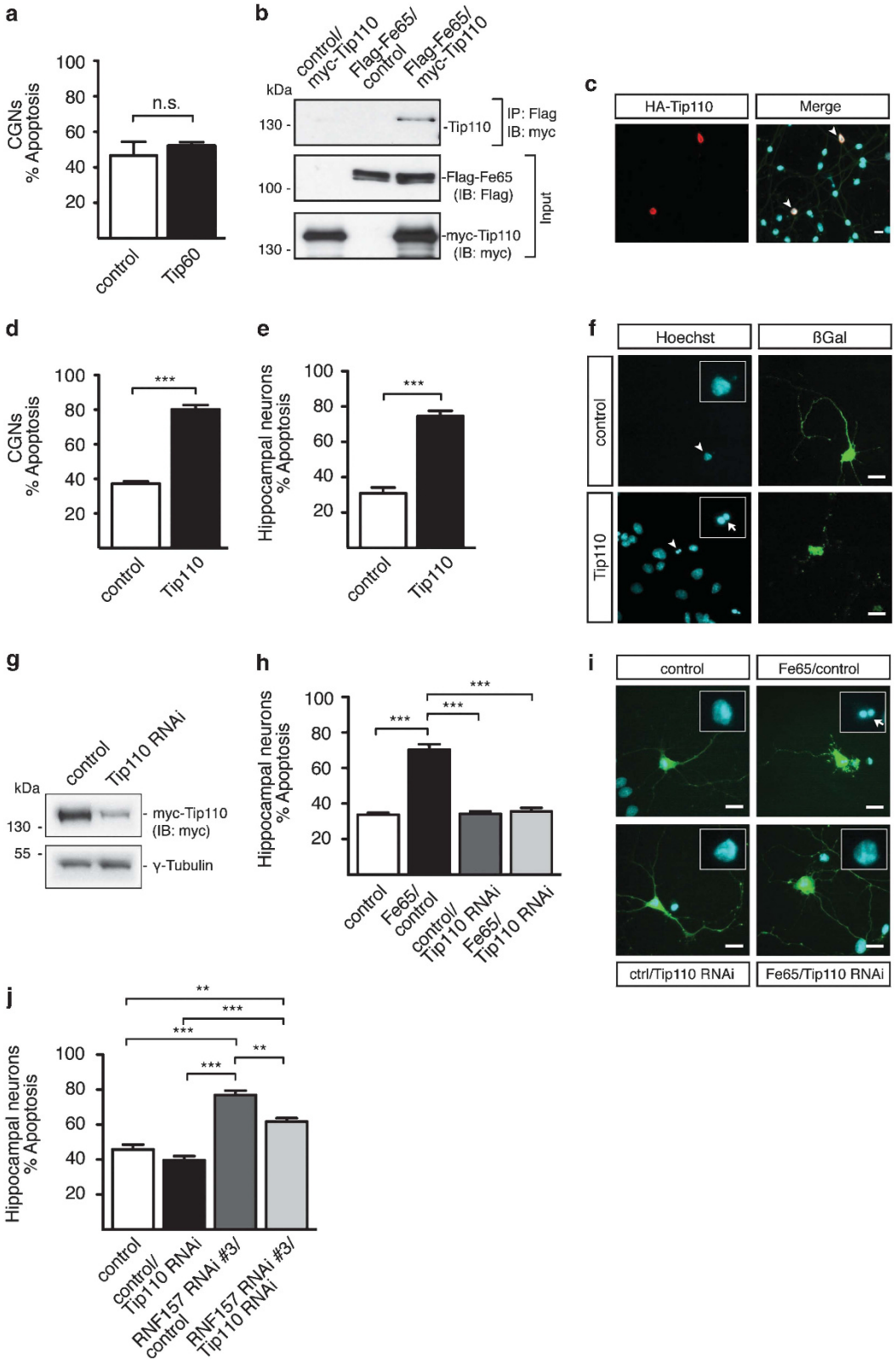

Figure 8 For caption see next page

Figure 8 Fe65 acts together with Tip110 in the control of neuronal apoptosis. (**a**) CGNs, transfected at DIV2 with control vector and the Tip60 expression plasmid, were analyzed at DIV6. A total of 2434 neurons from six independent experiments were included in the analysis (Mann–Whitney *U*-test, NS, nonsignificant, mean +S.E.M.). (**b**) Lysates of HEK293T cells, transfected with indicated plasmids, were subjected to immunoprecipitation with the Flag antibody, followed by immunoblotting with the myc antibody. (**c**) CGNs were transfected with the HA-Tip110 plasmid and subjected to immunostaining with the HA-antibody and the DNA dye bisbenzimide. Arrowheads indicate transfected neurons. Scale bar = 10 μm. (**d**) CGNs were transfected at DIV2 with control plasmid or the Tip110 expression plasmid together with the β-Gal plasmid, and analyzed at DIV6. A total of 541 neurons from three independent experiments were included in the analysis (Student's *t*-test, $^{***}P < 0.001$, mean +S.E.M.). (**e**) Hippocampal neurons were transfected at DIV2 with control plasmid or the Tip110 expression plasmid together with the β-Gal plasmid, and analyzed at DIV6. A total of 429 neurons from three independent experiments were included in the analysis (Student's *t*-test, $^{***}P < 0.001$, mean +S.E.M.). (**f**) Representative images of neurons in **8e**. Arrowheads indicate nuclei of transfected neurons and arrow indicates pyknotic nucleus. Insets depict higher magnification of nuclei. (**g**) Lysates of HEK293T cells transfected with the myc-Tip110 plasmid together with control vector and Tip110 RNAi were immunoblotted with the myc antibody or the γ-tubulin antibodies. The latter served as loading control. (**h**) Hippocampal neurons, transfected at DIV2 with control vectors, the Fe65 plasmid, the Tip110 RNAi plasmid or both the Fe65 and the Tip110 RNAi plasmids, were analyzed at DIV7 as described in **2c**. A total of 1447 neurons from four independent experiments were included in the analysis (ANOVA, $^{***}P < 0.001$, mean +S.E.M.). (**i**) Representative images of neurons in **8h**. Insets depict higher magnification of nuclei and arrow indicates pyknotic nucleus. Scale bar equals 20 μm. (**j**) Hippocampal neurons, transfected at DIV2 with control vectors, the Tip110 RNAi plasmid, the RNF157 RNAi #3 plasmid or both the Tip110 RNAi and the RNF157 RNAi #3 plasmids, were analyzed at DIV7 as described in **2c**. A total of 1410 neurons from four independent experiments were included in the analysis (ANOVA, $^{**}P < 0.01$, $^{***}P < 0.001$, mean +S.E.M.)

Conflict of Interest

The authors declare no conflict of interest.

Acknowledgements. We thank C Mukherjee and S Vingill for critical reading of the manuscript, and C Imig for help at the initial phase of the study. This work was supported by the Max Planck Society, the Deutsche Forschungsgemeinschaft (STE1117/5-1, GO1092-1/2 and -2/1), the Cluster of Excellence and DFG Research Center for Nanoscale Microscopy and Molecular Physiology of the Brain (CNMPB), Göttingen, and an the Excellence Stipend of the University of Göttingen (to S-JL).

1. Lennox G, Lowe J, Morrell K, Landon M, Mayer RJ. Ubiquitin is a component of neurofibrillary tangles in a variety of neurodegenerative diseases. *Neurosci Lett* 1988; **94**: 211–217.
2. Lowe J, Blanchard A, Morrell K, Lennox G, Reynolds L, Billett M *et al.* Ubiquitin is a common factor in intermediate filament inclusion bodies of diverse type in man, including those of Parkinson's disease, Pick's disease, and Alzheimer's disease, as well as Rosenthal fibres in cerebellar astrocytomas, cytoplasmic bodies in muscle, and mallory bodies in alcoholic liver disease. *J Pathol* 1988; **155**: 9–15.
3. Mayer RJ, Lowe J, Lennox G, Doherty F, Landon M. Intermediate filaments and ubiquitin: a new thread in the understanding of chronic neurodegenerative diseases. *Prog Clin Biol Res* 1989; **317**: 809–818.
4. McKinnon C, Tabrizi SJ. The ubiquitin-proteasome system in neurodegeneration. *Antioxidants Redox Signal* 2014P.
5. Dennissen FJ, Kholod N, van Leeuwen FW. The ubiquitin proteasome system in neurodegenerative diseases: culprit, accomplice or victim? *Prog Neurobiol* 2012; **96**: 190–207.
6. Hershko A, Ciechanover A. The ubiquitin system. *Annu Rev Biochem* 1998; **67**: 425–479.
7. Chen ZJ, Sun LJ. Nonproteolytic functions of ubiquitin in cell signaling. *Mol Cell* 2009; **33**: 275–286.
8. Ikeda F, Dikic I. Atypical ubiquitin chains: new molecular signals. 'Protein MODIFICATIONS: BEYOND THE USUAL SUspects' review series. *EMBO Rep* 2008; **9**: 536–542.
9. Deshaies RJ, Joazeiro CA. RING domain E3 ubiquitin ligases. *Annu Rev Biochem* 2009; **78**: 399–434.
10. Li W, Bengtson MH, Ulbrich A, Matsuda A, Reddy VA, Orth A *et al.* Genome-wide and functional annotation of human E3 ubiquitin ligases identifies MULAN, a mitochondrial E3 that regulates the organelle's dynamics and signaling. *PLoS One* 2008; **3**: e1487.
11. Kitada T, Asakawa S, Hattori N, Matsumine H, Yamamura Y, Minoshima S *et al.* Mutations in the parkin gene cause autosomal recessive juvenile parkinsonism. *Nature* 1998; **392**: 605–608.
12. Bomont P, Cavalier L, Blondeau F, Ben Hamida C, Belal S, Tazir M *et al.* The gene encoding gigaxonin, a new member of the cytoskeletal BTB/kelch repeat family, is mutated in giant axonal neuropathy. *Nature genetics* 2000; **26**: 370–374.
13. Chu J, Hong NA, Masuda CA, Jenkins BV, Nelms KA, Goodnow CC *et al.* A mouse forward genetics screen identifies LISTERIN as an E3 ubiquitin ligase involved in neurodegeneration. *Proc Natl Acad Sci USA* 2009; **106**: 2097–2103.
14. Balastik M, Ferraguti F, Pires-da Silva A, Lee TH, Alvarez-Bolado G, Lu KP *et al.* Deficiency in ubiquitin ligase TRIM2 causes accumulation of neurofilament light chain and neurodegeneration. *Proc Natl Acad Sci USA* 2008; **105**: 12016–12021.
15. He L, Lu XY, Jolly AF, Eldridge AG, Watson SJ, Jackson PK *et al.* Spongiform degeneration in mahoganoid mutant mice. *Science* 2003; **299**: 710–712.
16. Vorum H, Liu X, Madsen P, Rasmussen HH, Honore B. Molecular cloning of a cDNA encoding human calumenin, expression in *Escherichia coli* and analysis of its Ca2+-binding activity. *Biochim Biophys Acta* 1998; **1386**: 121–131.
17. Matagne A, Joris B, Frere JM. Anomalous behaviour of a protein during SDS/PAGE corrected by chemical modification of carboxylic groups. *Biochem J* 1991; **280**: 553–556.
18. Konishi Y, Stegmuller J, Matsuda T, Bonni S, Bonni A. Cdh1-APC controls axonal growth and patterning in the mammalian brain. *Science* 2004; **303**: 1026–1030.
19. Minopoli G, Gargiulo A, Parisi S, Russo T. Fe65 matters: new light on an old molecule. *IUBMB life* 2012; **64**: 936–942.
20. McLoughlin DM, Miller CC. The FE65 proteins and Alzheimer's disease. *J Neurosci Res* 2008; **86**: 744–754.
21. Ciechanover A, Orian A, Schwartz AL. Ubiquitin-mediated proteolysis: biological regulation via destruction. *Bioessays* 2000; **22**: 442–451.
22. Peng J, Schwartz D, Elias JE, Thoreen CC, Cheng D, Marsischky G *et al.* A proteomics approach to understanding protein ubiquitination. *Nature biotechnology* 2003; **21**: 921–926.
23. Pickart CM. Ubiquitin in chains. *Trends Biochem Sci* 2000; **25**: 544–548.
24. Saeki Y, Kudo T, Sone T, Kikuchi Y, Yokosawa H, Toh-e A *et al.* Lysine 63-linked polyubiquitin chain may serve as a targeting signal for the 26S proteasome. *EMBO J* 2009; **28**: 359–371.
25. Cao X, Sudhof TC. A transcriptionally [correction of transcriptively] active complex of APP with Fe65 and histone acetyltransferase Tip60. *Science* 2001; **293**: 115–120.
26. Liu Y, Li J, Kim BO, Pace BS, He JJ. HIV-1 Tat protein-mediated transactivation of the HIV-1 long terminal repeat promoter is potentiated by a novel nuclear Tat-interacting protein of 110 kDa, Tip110. *J Biol Chem* 2002; **277**: 23854–23863.
27. Liu Y, Lee MR, Timani K, He JJ, Broxmeyer HE. Tip110 maintains expression of pluripotent factors in and pluripotency of human embryonic stem cells. *Stem Cells Dev* 2012; **21**: 829–833.
28. Liu Y, Timani K, Ou X, Broxmeyer HE, He JJ. C-MYC controlled TIP110 protein expression regulates OCT4 mRNA splicing in human embryonic stem cells. *Stem Cells Dev* 2013; **22**: 689–694.
29. Liu Y, Timani K, Mantel C, Fan Y, Hangoc G, Cooper S *et al.* TIP110/p110nrb/SART3/p110 regulation of hematopoiesis through CMYC. *Blood* 2011; **117**: 5643–5651.
30. Timani KA, Liu Y, He JJ. Tip110 interacts with YB-1 and regulates each other's function. *BMC Mol Biol* 2013; **14**: 14.
31. Liu Y, Kim BO, Kao C, Jung C, Dalton JT, He JJ. Tip110, the human immunodeficiency virus type 1 (HIV-1) Tat-interacting protein of 110 kDa as a negative regulator of androgen receptor (AR) transcriptional activation. *J Biol Chem* 2004; **279**: 21766–21773.
32. Koga M, Komatsu N, Kawamoto N, Shichijo S, Itoh K, Yamada A. Analysis of cellular localization of SART3 tumor antigen by a newly established monoclonal antibody: heterotopic expression of SART3 on the surface of B-lineage leukemic cells. *Oncol Rep* 2004; **11**: 785–789.
33. Guenette SY, Chen J, Jondro PD, Tanzi RE. Association of a novel human FE65-like protein with the cytoplasmic domain of the beta-amyloid precursor protein. *Proc Natl Acad Sci USA* 1996; **93**: 10832–10837.
34. Ando K, Iijima KI, Elliott JI, Kirino Y, Suzuki T. Phosphorylation-dependent regulation of the interaction of amyloid precursor protein with Fe65 affects the production of beta-amyloid. *J Biol Chem* 2001; **276**: 40353–40361.
35. Guenette S, Chang Y, Hiesberger T, Richardson JA, Eckman CB, Eckman EA *et al.* Essential roles for the FE65 amyloid precursor protein-interacting proteins in brain development. *EMBO J* 2006; **25**: 420–431.
36. Cheung HN, Dunbar C, Morotz GM, Cheng WH, Chan HY, Miller CC *et al.* FE65 interacts with ADP-ribosylation factor 6 to promote neurite outgrowth. *FASEB J* 2014; **28**: 337–349.
37. Lu C, Pribanic S, Debonneville A, Jiang C, Rotin D. The PY motif of ENaC, mutated in Liddle syndrome, regulates channel internalization, sorting and mobilization from subapical pool. *Traffic* 2007; **8**: 1246–1264.
38. Bilimoria PM, Bonni A. Cultures of cerebellar granule neurons. *CSH Protocols* 2008; **2008**: pdb prot 5107.
39. Goslin K, Asmussen H, Banker G. Rat hippocampal neurons in low-density cultures. *Culturing Nerve Cells*. The MIT Press: Cambridge MA, USA, 1998; **1998**: pp 339–370.
40. Stoppini L, Buchs PA, Muller D. A simple method for organotypic cultures of nervous tissue. *J Neurosci Methods* 1991; **37**: 173–182.

Supplementary Information accompanies this paper on Cell Death and Differentiation website (http://www.nature.com/cdd)